High Contrast Imaging Through Scattering Media Using Structured Illumination Fourier Filtering

David Frantz
Supervisor: Dr. Edouard Berrocal
2017

Master's thesis in Engineering Physics

LUND UNIVERSITY

Division of Combustion Physics
Faculty of Engineering, LTH

Abstract

In imaging, obtaining high contrast is of great importance. When imaging through scattering media, optical filtering techniques are used to filter out multiple light scattering which causes loss of contrast. Imaging through scattering media is used in Bio-Medicine when looking through human skin; in characterization of spray systems in Combustion Engineering as well as in other applications where visualization within fog, smoke or turbid water is necessary. This project focuses on the development of a novel optical filtering method called Structured Illumination Fourier filtering, or SIF. It is shown here that SIF can achieve high contrast imaging using visible light through a scattering medium of optical depth up to OD = 15. Measurements are performed through a water dispersion of polystyrene spheres of D = 0.13 µm. The performance of SIF is compared to the individual performances of Fourier filtering and Structured Illumination. SIF is shown to outperform these techniques in optical depths above OD = 10. A common way to increase contrast through a given scattering medium with small particles is to use a longer wavelength. It is shown here that SIF can achieve equally high contrast through a medium using blue, green and red light. Also, a comparison between the recorded images and simulations from the newly developed online Monte Carlo software Multi-Scat[1] shows great promise for the validation of the software.

General summary of the content of the thesis

Structured Illumination Fourier filtering(SIF) is an optical filtering technique for high contrast imaging through scattering media. Scattering media is a term that describes media that scatter light strongly but does not absorb well. Imaging through a scattering medium is challenging since multiple scattering can, depending on the optical properties, reduce contrast strongly. The optical properties of a scattering medium can be described by its optical depth(OD) and its scattering phase function. The OD is the average number of scattering events that occur for photons crossing the medium. The phase function describes in which angles photons are scattered. The experiments in this project cover $2.20 \leq \mathrm{OD} \leq 15.00$ with near isotropic phase functions.

SIF is a combination of two optical filtering techniques used in the trans-illumination detection mode: Structured Illumination(SI) and Fourier filtering(FF). Structured Illumination uses a periodic modulation to mark in-focus light. Three images with a phase-shift in the modulation is used to create the full image in a way that discriminates multiple light scattering. Optical Fourier filtering also discriminates against multiple light scattering by blocking high spatial frequencies, which contain a higher-than-average portion of scattered to non-scattered light.

The contrasts achieved using SI, FF and SIF are quantified through the modulation transfer function(MTF). For this purpose a Matlab code calculating the MTF from a single image of a sector star has been created. The comparison between the methods show that SIF provides greatly improved contrast compared to either SI or FF when imaging through high OD:s($10 < \mathrm{OD} \leq 15$). Through lower OD:s the benefits of SIF are not as apparent. Some results are also compared to a simulation performed with an online Monte Carlo software developed by J.Jönsson and Dr. E.Berrocal at Lund University. The comparison contributes to the validation of the software.

Abbreviations

FF - (optical) Fourier filtering

FT - Fourier transform

MC - Monte Carlo method

MTF - Modulation Transfer Function

OD - Optical depth

p-p - post-processing

RGB - red-green-blue

SI - Structured Illumination

SIF - Structured Illumination Fourier filtering

Contents

1 Introduction **1**

2 Light propagation through scattering media **2**
2.1 Optical depth . . . 2
2.2 Scattering phase function . . . 3
2.3 Monte Carlo simulation . . . 5

3 Optical filtering strategies **6**
3.1 Structured Illumination . . . 6
3.2 Optical Fourier filtering . . . 9
3.3 Combining Structured Illumination and Fourier filtering . . . 11

4 Quantifying image contrast **12**
4.1 Modulation Transfer Function . . . 12
4.2 Calculating the MTF from the Fourier domain . . . 13

5 Image post-processing and MTF calculations **14**
5.1 Residual lines suppression in structured illumination . . . 14
5.2 Description of the MTF Matlab code . . . 16
5.3 MTF calculation comparison . . . 18
5.4 MTF of FF and SI for an Example of Turbid Water . . . 18
5.5 Effect of residual lines suppression on the MTF . . . 19

6 Experimental setup **20**
6.1 Description of the optical setup . . . 20
6.2 Description of the measurements . . . 23

7 Experimental results and discussion **24**
7.1 Effect of optical depth . . . 24
7.2 Effect of illumination wavelength . . . 27
7.3 Comparison between two objectives for Fourier filtering . . . 31

8 Multi-Scat Monte Carlo simulation **32**
8.1 The Multi-Scat software . . . 32
8.2 Input parameters of the simulation . . . 34
8.3 Simulation validation . . . 34

9 Conclusions and outlook **37**

Appendices **40**

A MTF comparison for all imaged cases **40**

B Mathematics of Structured Illumination **44**

1 Introduction

•Background

Since the invention of the modern camera in the early 19:th century, imaging has been one of the most important ways of measuring quantities in almost all fields of research. A definition of imaging might be to record some properties of an object, and its geometrical characteristics, by collecting its scattered or emitted electromagnetic radiation. This definition includes regular camera systems, but also includes the human eye, x-ray machines, MRI:s, modern telescopes and much more. A key aspect in imaging is the concept of contrast. Contrast is a measure of intensity or color difference, which makes details visible[2, p. 579]. Good image contrast is crucial for accurate measurements. For example, an image of objects in a dark room will be hardly visible because the contrast between bright and dark areas is low. Likewise, contrast will be low when imaging through a scattering medium. Some examples of scattering media are: fog, smoke, clouds, turbid liquids and medical tissue.

Scattering and absorption are the two main light-matter interactions by which we perceive the world around us. Absorption interactions cause a reduction of propagating light energy while scattering interactions cause a redistribution of propagation direction. An imaging system collects light that is scattered by an object and uses the information carried by the light to construct an image of the object. Only a part of that light is however scattered off of the surface of the object. The rest of the light enters the object and is being scattered multiple times and/or is absorbed in interactions with the inner structure of the object. Some light is scattered backwards and leaves the object in the reverse direction. This light is also collected by the imaging system. Information about shape and structure is connected to the propagation direction of light and is therefore lost by multiple light scattering. The contrast of the image created by the imaging system is therefore reduced by the collection of the multiply scattered light[3, p. 3-6].

In classical imaging the light illuminating the object of interest and is being collected is typically ambient. Ambient lighting, such as generated from a ceiling lamp or the sun, is a light source located far from the object, illuminating everything around it. In research the illumination source is often controlled. Thus, a lamp or a laser beam is specifically aimed at the object of interest, yielding local illumination. In such case, three common detection modes can be used: backscatter detection, side-scatter detection and trans-illumination detection. An example of backscatter detection is the flash of a camera which is being reflected back. The side-scatter detection mode is the most common detection mode when imaging surrounding objects. However, in trans-illumination detection the light source is positioned behind the object, creating a shadow. The recorded image will, as opposed to ambient, side- and backscatter illumination, be dark at the location of the object and bright around it. If the illumination light is scattered before it reaches the image recorder, dark areas may become brighter and bright areas darker, resulting in contrast loss. This is the case when imaging in or through a scattering medium.

•Goal of this project

To counter the effect of contrast loss by scattering in trans-illumination detection, various techniques for filtering out scattered light can be applied. Examples of filtering techniques are time gating[4, 5], polarization filtering[6], Fourier filtering[7, 8] and Structured Illumination[9]. A proof-of-concept article, published in 2016 by E. Berrocal et al. in Optics Letters [10], showed that Structured Illumination and Fourier filtering can be combined, resulting in an enhanced filtering effect. This project focuses on the development of the novel technique, named SIF, and further studies the combined contrast enhancing effect of Structured Illumination and Fourier filtering. A trans-illumination optical setup is developed and used for imaging through scattering media of different turbidities and with different illumination wavelengths. The contrast of the images is calculated using a Matlab code, developed as part of the project, for calculation of MTF from an image of a sector star. In addition

to investigating SIF, the images will be used to compare simulation results from an online Monte Carlo software, developed by J.Jönsson and Dr. E.Berrocal at Lund University, with experimental data.

•Disposition

Sections 2-4 provides the reader with relevant information about light propagation through scattering media, the Monte-Carlo method, optical filtering techniques and how to quantify image contrast. A basic knowledge of these fields is necessary to assimilate the content of the later sections. Section 5 describes the post-processing and data analysis methods which have been developed and implemented for this project. The experimental results are presented and discussed in section 7. In section 8 the Multi-Scat software[1] is described and the experimental measurements are compared to corresponding simulations. In section 9 the conclusions of this work is summarized and an outlook to suggested future work is done.

2 Light propagation through scattering media

This section describes the characteristics of scattering media and the concepts used to define their optical properties. From these properties light propagation in the medium can be characterized. The last part briefly explains how those optical properties is used in a Monte Carlo model of light propagating through scattering media.

2.1 Optical depth

Light which enters or leaves a homogeneous medium will be scattered at the surfaces because of the change in refractive index. If the medium is not homogeneous however, interactions may occur inside the medium at inhomogeneities forming scattering centers. The interactions may be either scattering or absorption. Because of these interactions, the light intensity will attenuate as a function of the distance into the medium. The combined effect of scattering and absorption is therefore called extinction [11, p. 64-65].

In the context of this report, a scattering medium refers to a medium which has scattering centers that scatters light strongly but does not absorb well. Combined, these two characteristics enable light to scatter multiple times, loosing all direction, without loosing its total power. In this type of media, light which enters from one side, may scatter multiple times and escape the medium in all directions, causing a glowing effect. Examples of scattering media are clouds, fog, milk and tissue. In clouds and fog, the scattering centers are approximately spherical water droplets. In this project scattering centers are considered to be spherical particles.

The strength of scattering and absorption from spherical particles is defined by their cross-sections. The cross-sections typically depend on wavelength, material and particle size. The scattering cross-section describes the area on which the incident light energy equals the total energy scattered by the scattering center. Similarly, the absorption cross-section is the area on which the incident energy equals the absorbed energy [11, p. 65]. In other words, the cross-sections describe the interaction area of a single spherical particle. Eq.1 defines the extinction cross-section as the sum of the scattering and absorption cross-sections.

$$\sigma_e = \sigma_s + \sigma_a \tag{1}$$

σ_s and σ_a are the cross-sections for scattering and absorption respectively. In a typical scattering medium σ_s is the dominant term. The extinction coefficient describes the extinction per unit length in a medium and is defined as

$$\mu_e = N \times \sigma_e, \tag{2}$$

where N is the particle number density, i.e. particles/volume. The total extinction of a medium of defined size can be described by its optical depth(OD). The optical depth approximately equals the average number of interaction events that occur for light crossing the medium. It is defined as

$$OD = \mu_e \times L, \tag{3}$$

where L is the length of the medium in the propagation direction. The scattering order is the actual amount of scattering events that has occurred for a photon. The scattering orders of light penetrating a medium are distributed around a peak approximately at the OD [11, p. 64-74]. The higher optical depth a medium has, the smaller is the portion of light which has not been scattered. Optical filtering is used to filter out the multiply scattered light, thus increasing the ratio of unscattered-to-multiply scattered light intensity. The larger this ratio is, the better is the image contrast.

2.2 Scattering phase function

Scattering is not fully described by the number of scattering events. Another important characteristics is in which angles light is scattered. The effect of scattering angle on contrast in imaging through scattering media is twofold. If the scattering in a medium is isotropic, very little light carry any information and so most of the detected light is perceived as noise. Imaging through such media quickly lose contrast with increasing OD but details remain sharp. In a medium where light is mostly scattered in the forward direction, more light carry some information. Such scattering introduces image blur but more contrast is preserved through higher optical depths.

The Lorenz-Mie theory is the solution to Maxwell's equations for a plane wave interacting with a spherical particle. Simplified, the solution is an intensity distribution as a function of scattering angle, called the scattering phase function. According to the theory, the ratio of particle diameter and wavelength is an important factor in deciding the scattering phase function. Small ratios scatter more isotropically while large ratios scatter mostly in the forward direction [3, p. 11-12, 28-39, 114-130]. Figures 1a and 1e show the scattering phase functions for blue($\lambda = 473$ nm) and red($\lambda = 671$ nm) light, scattering off of spherical particles with D = 0.13 µm. Since 130/473 = 0.275 and 130/671 = 0.194, both red and blue light scatter somewhat isotropically but red light at a higher degree. Figures 1b and 1f show the scattering phase functions for the same wavelengths scattering off of spherical particles with D = 5 µm. Since 5000/473 = 10.57 and 5000/671 = 7.45, both red and blue light scatter much more in the forward direction in this case. Figure 1 also includes phase functions for green($\lambda = 532$ nm) light and the captions include the scattering cross-sections for all cases. Figure 2 shows an example of the effect of scattering from particles smaller than the wavelength when imaging through clean and turbid water.

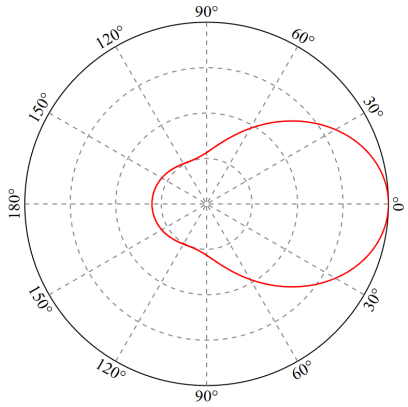

(a) $\lambda = 473$ nm, D $= 0.13$ µm, $\sigma_s = 6.51 \times 10^{-10}$ mm^2

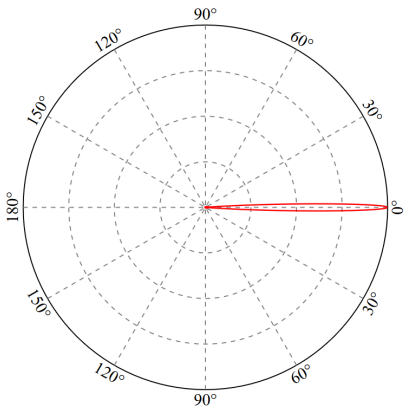

(b) $\lambda = 473$ nm, D $= 5$ µm, $\sigma_s = 4.74 \times 10^{-5}$ mm^2

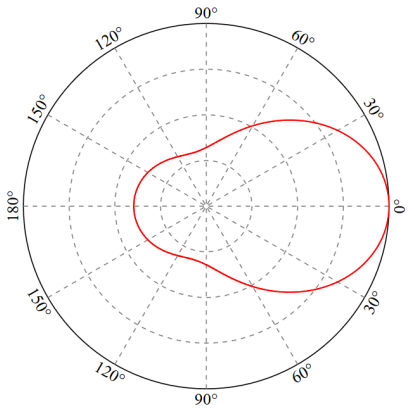

(c) $\lambda = 532$ nm, D $= 0.13$ µm, $\sigma_s = 4.43 \times 10^{-10}$ mm^2

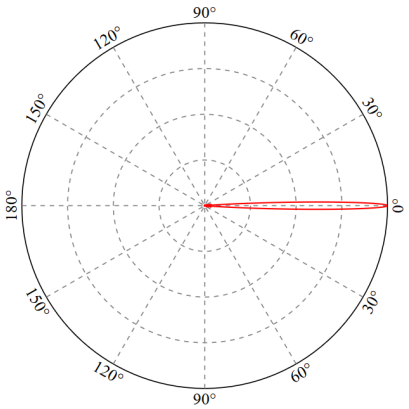

(d) $\lambda = 532$ nm, D $= 5$ µm, $\sigma_s = 3.87 \times 10^{-5}$ mm^2

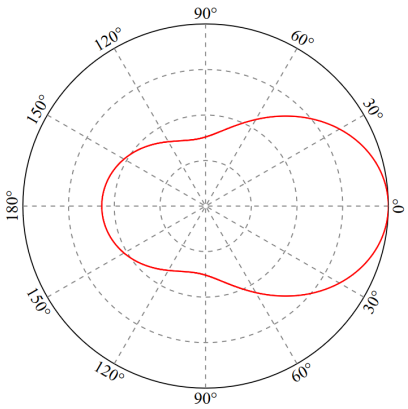

(e) $\lambda = 671$ nm, D $= 0.13$ µm, $\sigma_s = 1.86 \times 10^{-10}$ mm^2

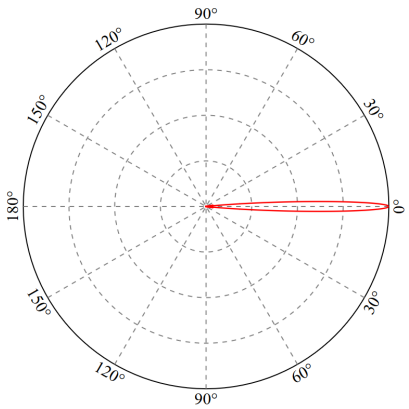

(f) $\lambda = 671$ nm, D $= 5$ µm, $\sigma_s = 4.83 \times 10^{-5}$ mm^2

Figure 1: Scattering phase functions for blue($\lambda = 473$ nm), green($\lambda = 532$ nm) and red($\lambda = 671$ nm) light interacting with spherical particles with D $= 0.13$ µm and D $= 5$ µm. Note how the scattering cross-section varies strongly with wavelength for the smaller particles, but not for the larger. Figures created using the Multi-Scat software from [1]

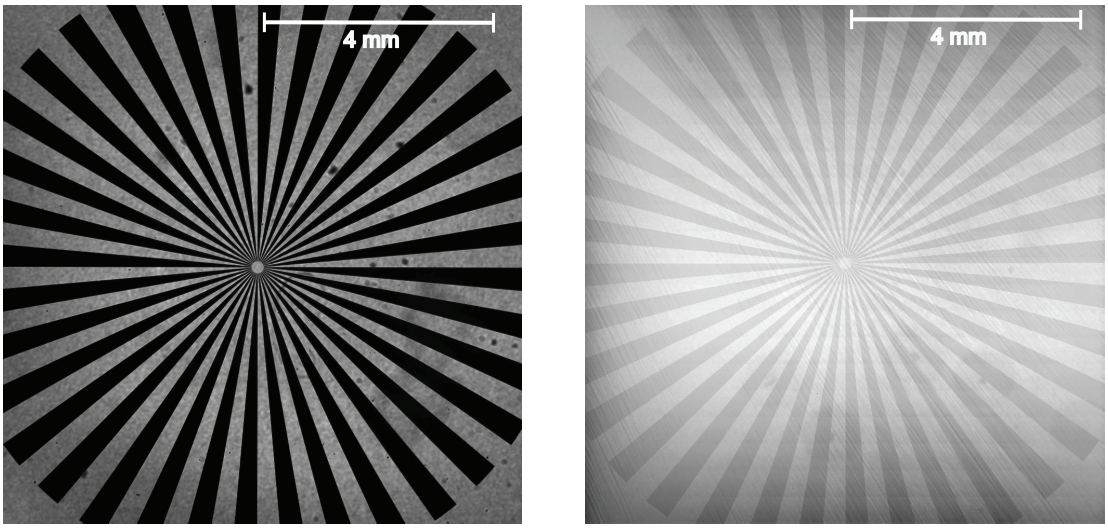

(a) Imaging through clean water.

(b) Imaging through turbid water.

Figure 2: Comparison between images recorded through clean and turbid water. The contrast is strongly reduced when imaging through the turbid water, making the imaged star target less visible.

2.3 Monte Carlo simulation

The Monte Carlo (MC) method is a powerful tool for simulating physical processes using random numbers. It is suitable for processes which can be viewed as stochastic, such as photon transport. A Monte Carlo simulation tracks individual photons, or weighted photon packets, as they propagate through a virtual medium. The path length for a photon packet between two interactions with the medium is calculated by

$$l_{fp} = -\frac{ln\xi}{\mu_e}, \tag{4}$$

where $|\xi| \leq 1$, is a random number. If the calculated path length leads to an interaction outside the medium, the photon packet does not interact. If the path length ends inside the medium an interaction occur. In an interaction a fraction of the packet, based on the relative strengths of scattering and absorption, is absorbed. The rest is scattered in a new propagation direction, based on the appropriate scattering phase function. Thus, a second random number is used with the cumulative probability depth function(CPDF) of the scattering phase function. It decides in which angle the packet is scattered in the plane of incidence. A third random number decides the angle in the third dimension. This process is repeated until the photon packet has left the virtual medium or is fully absorbed. With billions of tracked packets the simulation results get statistical relevance and provides a good approximation of the real physical process [11, p. 90-97].

Figure 3 shows an MC simulation of light penetrating a scattering medium of OD = 11.25 with particles of D = 0.4 µm. The images show the impact of scattering order on the contrast.

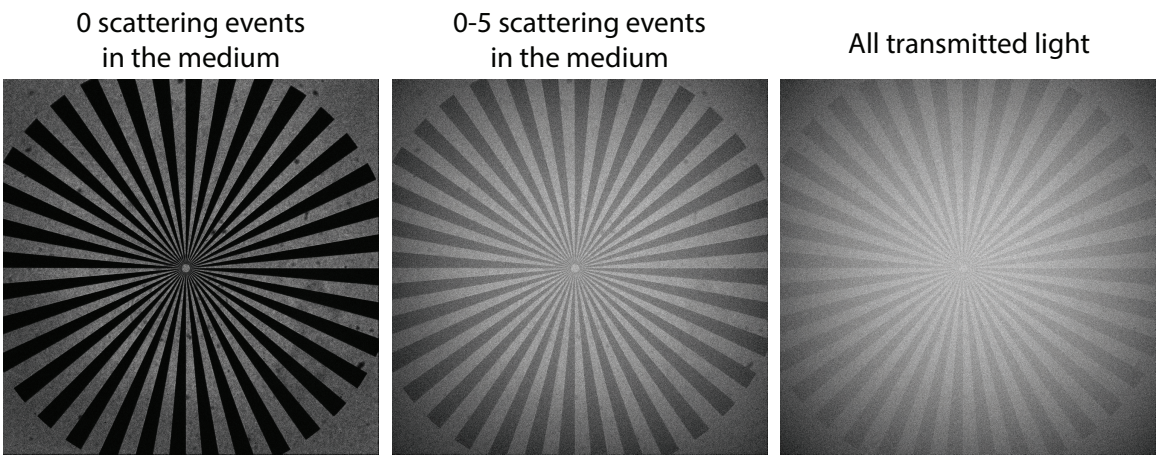

Figure 3: A simulation of scattering through a medium of OD = 11.25 with particles of D = 0.4 µm. The image contrast from all light is much lower than the contrast from the least scattered light. Since the particle size is relatively small, the scattering doesn't yield a blurry image. Simulation performed using [1].

3 Optical filtering strategies

In this section the optical filtering strategies of Structured Illumination and Fourier filtering are explained. The two first parts explain the two strategies individually. In the last part of the section their combination into SIF is discussed.

3.1 Structured Illumination

The basic working principle of Structured Illumination(SI) is to mark the in-focus light by imposing a recognizable structure onto it. This makes it possible to recognize and reject the out-of-focus light, such as the light that has been scattered multiple times, and thereby increase the contrast. The structured light can be obtained by letting a homogeneous beam profile illuminate a sinusoidal mask target of frequency f_{mod} along one direction. This leaves a striped light profile which then illuminates an object of which an image is formed. The image is formed by two components: the unscattered in-focus light that forms the exact image of the object together with the striped structure, and the scattered out-of-focus light that is responsible for blur and loss of contrast in the image(a setup is shown in Figure 4). The filtering is performed by taking three images with the structure mask shifted $2\pi/3$ radians along its modulation direction between each image, denoted I_0, I_{120} and I_{240}. In the blurred component of the images, the shifted structure will not be visible as it is only composed of out-of-focus light. Therefore, this component is equivalent for all three images and can be removed via subtraction. By implementing

$$I_{SI} = \frac{\sqrt{2}}{3}\sqrt{(I_0 - I_{120})^2 + (I_0 - I_{240})^2 + (I_{120} - I_{240})^2}, \tag{5}$$

a full image can be constructed from the three structured images [12, p. 47-51]. An example of this is shown in Figure 5. Figure 4 illustrates an optical setup used for Structured Illumination. Theoretically, three shifted images are enough to perfectly construct the full image with no trace of the structure lines [10]. In fact, Eq.5 is true for all modulations of higher orders of the base frequency f_{mod}, except for $3nf_{mod}$ frequencies which cancels to zero. A calculation verifying this is included in appendix B. This suggests that nearly any periodic modulation can be used, such as a square or a saw-tooth modulation. Figure 6 shows how a one-dimensional constant(I=1) can be constructed

from three modulated versions of the constant using either a sinusoidal or a square modulation and appropriate scaling factors.

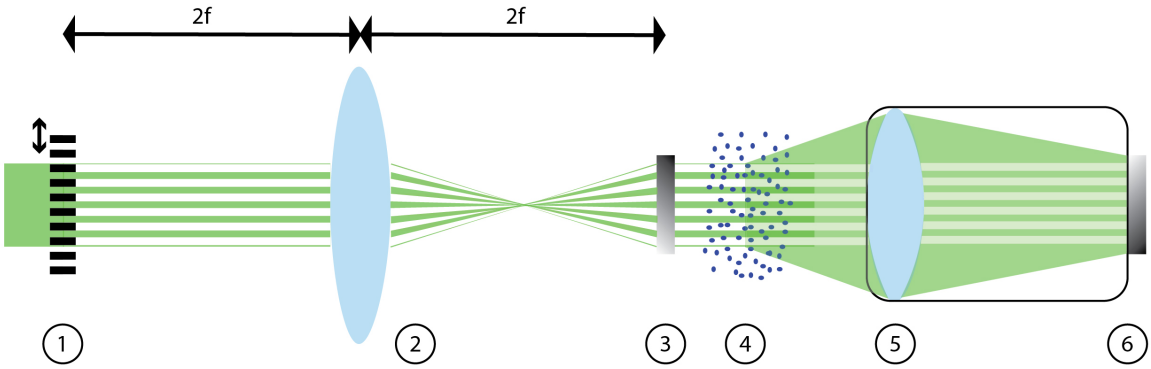

Figure 4: Illustration of an optical setup for Structured Illumination. A beam is modulated by a movable Ronchi or sinusoidal grating(1). The modulated beam is imaged by a lens(2) onto the object of interest(3). The illuminated object is then imaged through a scattering medium(4), using an objective lens, which forms an image(5) on a detector array(6).

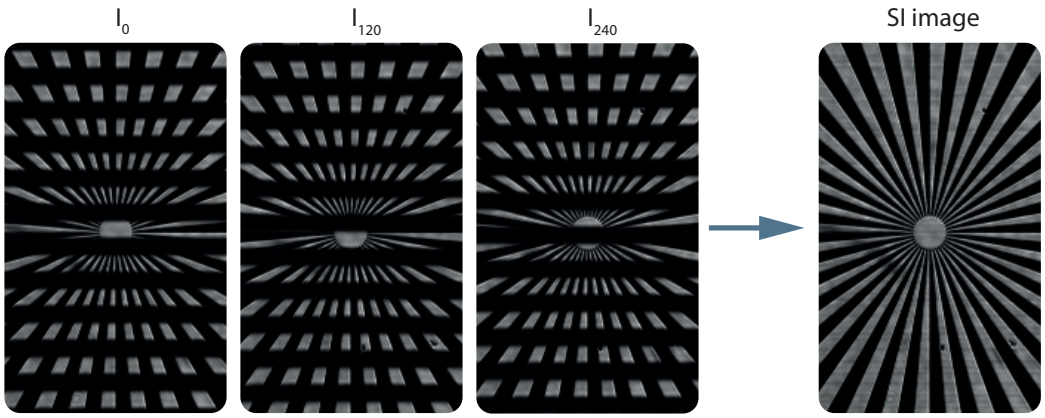

Figure 5: Three structure illumination sub-images, phase-shifted 0°, 120° and 240° combining into a full image.

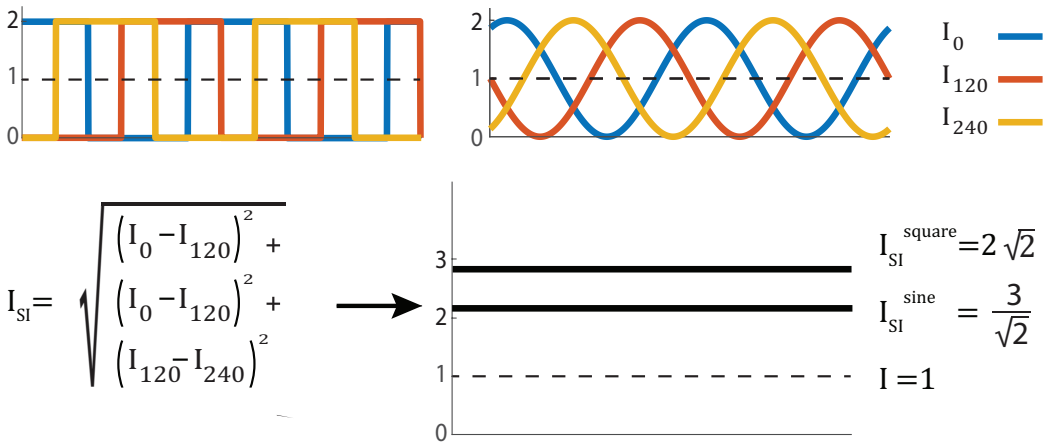

Figure 6: Illustration of three sinusoidal and square modulations of the constant I=1, being combined using Eq.5(without scaling factor) into scaled constants I_{SI}. These constants are used to properly scale the resulting SI image.

Figure 7 shows how the modulation falls out-of-focus in multiply scattered components of the illumination. Since the modulation is no longer visible in the twice scattered component, that component and components of higher scattering order will be removed when applying Eq.5.

When illuminating through an optically dense scattering medium, the in-focus to out-of-focus light ratio will become very low. At some optical depth, the in-focus light intensity is lower than the noise level. At this point the structure will no longer be visible making the filtering method no longer work. Figure 8 shows an image taken using SI next to the unfiltered image from Figure 2. The SI image has much higher contrast.

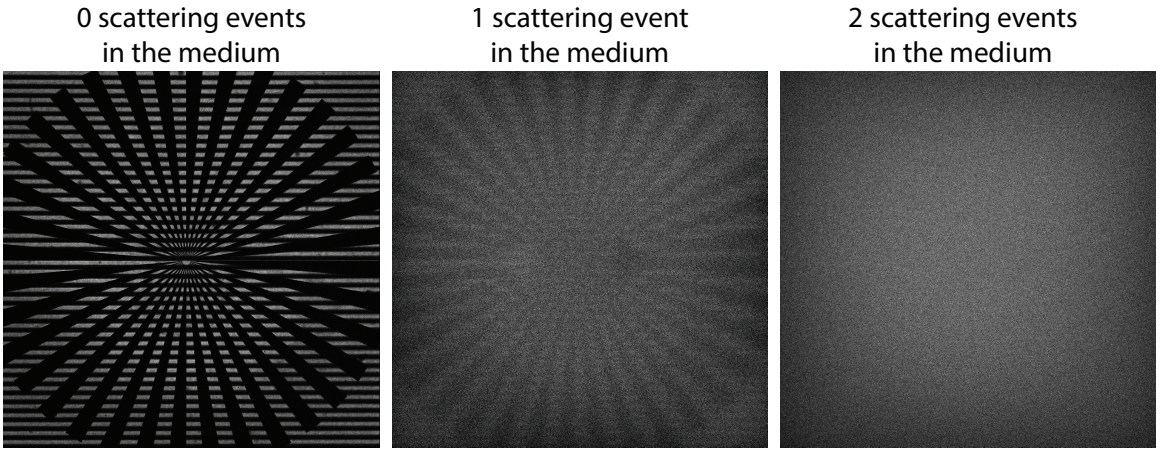

Figure 7: Results from Monte Carlo simulation using the Multi-Scat software[1]. The images show scattering order components of a modulated image having been scattered zero times, once and twice while propagating through a scattering medium. In the single scattering component the modulation is still vaguely visible.

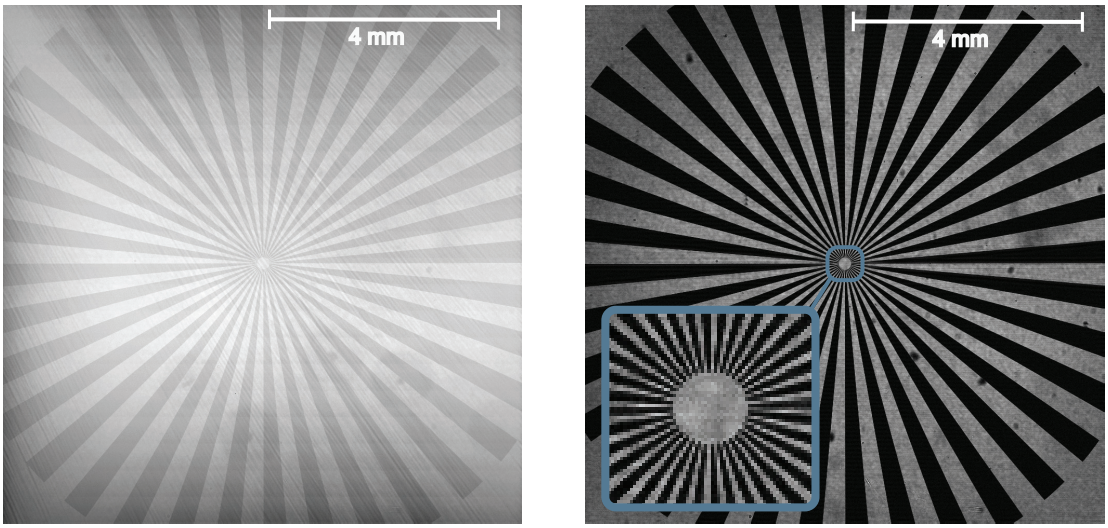

(a) Imaging through turbid water.

(b) SI filtered image.

Figure 8: Experimental images recorded through the same scattering medium without filtering and with SI. The images clearly show that the contrast is greatly increased when using SI.

3.2 Optical Fourier filtering

The first part of this section explains the Fourier component decomposition of light, and how it is used to optically perform Fourier filtering. The second part explains how the same principle is used to filter out scattered light.

•Optical Fourier filtering in imaging

Any periodic signal can be decomposed into a set of single frequency components of given amplitude, called the Fourier transform of the signal. Two-dimensional signals, such as images, can be decomposed into a set of single spatial frequencies, ν_x and ν_y in the x and y directions. The lower frequency components build up the broad structure of the field and the higher ones provide sharp edges and fine image details.

Consider a light field signal in the x-y plane, carrying the image information of an object, traveling in the z-direction. The Fourier transform components of such a field may be expressed in ν_x and ν_y coordinates with corresponding amplitudes. The components can be shown to be complex amplitudes in the x-y plane of plane waves traveling in directions with angles Θ_x and Θ_y to the y-z and x-z planes. The angles are defined in Eq.6, where λ is the wavelength of the light and ν_x and ν_y are the spatial frequencies in the x and y directions respectively [13, p. 103-108].

$$\Theta_x = sin^{-1}(\lambda\nu_x); \quad \Theta_y = sin^{-1}(\lambda\nu_y) \tag{6}$$

The lowest frequencies, ν_i close to 0, carries the mean intensity and is traveling along the z-axis and has uniform intensity in the x-y plane. Since the Fourier components are plane waves traveling with different angles, they will naturally spread out. The Fourier transform can therefore be observed by studying the complex amplitude of the light field in a plane adequately far away from the object. A lens can focus these components and form the Fourier transform in the focal plane of the lens. Low frequencies are focused in the center and the higher frequencies further out. Inserting a blocking mask in this Fourier plane will therefore optically Fourier filter(FF) the information in the light field. As an example, a low pass filter is implemented by blocking all components apart from the central

ones[13, p. 116-120]. In this project the Fourier filtering is performed in the Fourier plane of the imaging camera objective lens. A scheme of the Fourier filtering setup used is shown in Figure 9.

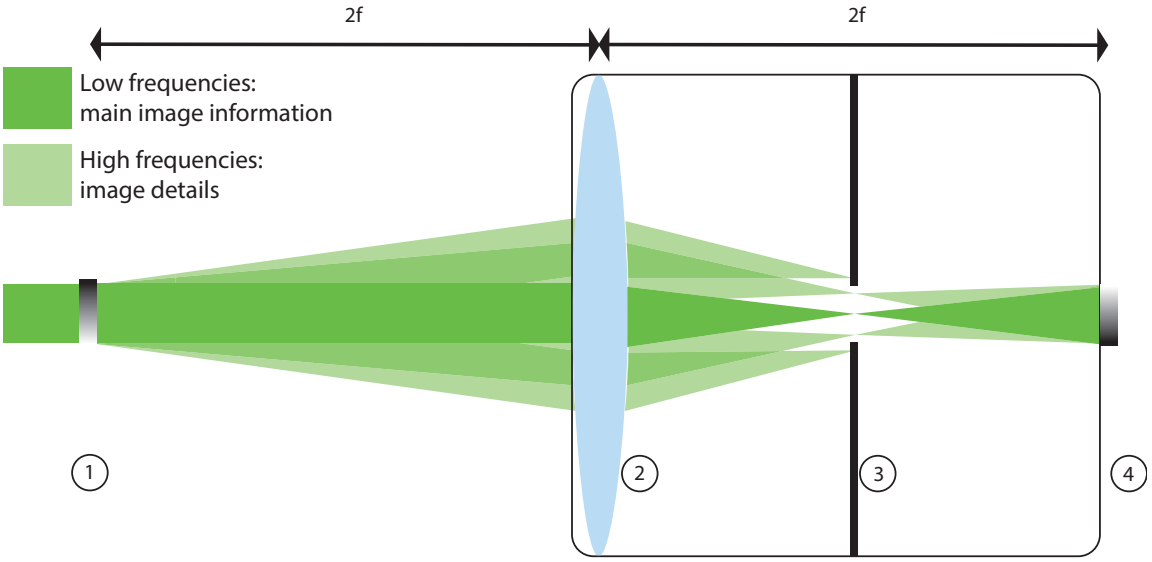

Figure 9: An illustration of the basis of optical Fourier filtering with an objective-aperture setup. An object(1) is illuminated and diffracts the light field into spatial frequency components. The objective lens(2) focuses the components in the Fourier plane(3), where high order components are blocked by an aperture. The transmitted components are imaged on a CCD array(4). The image is formed only by the lower frequency components.

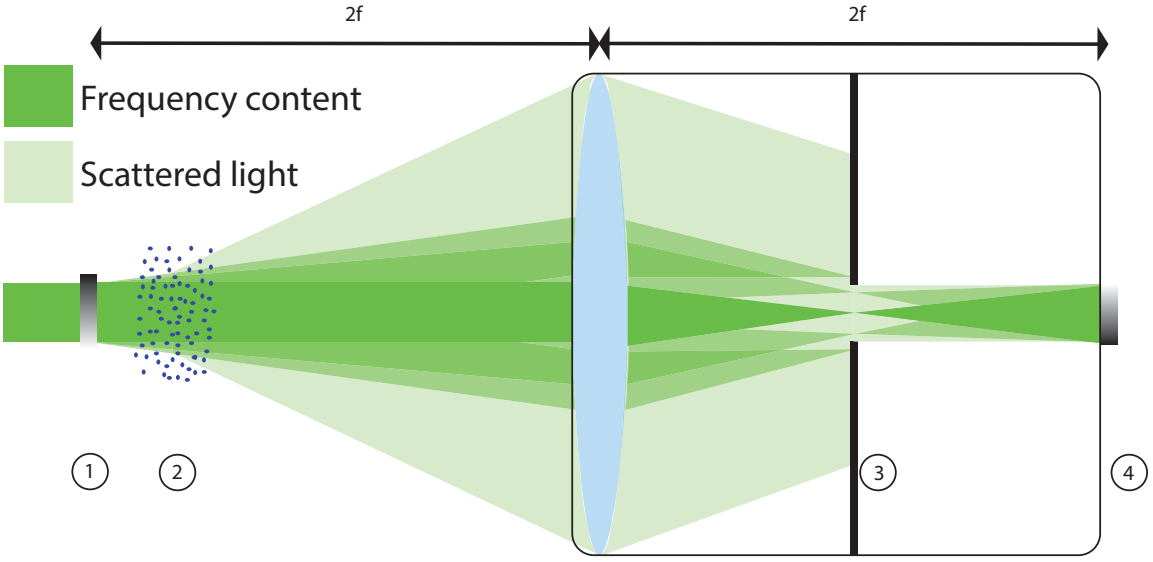

Figure 10: An illustration of Fourier filtering in scattering media. The light from the object(1) is scattered in a medium(2). Scattered light and high frequencies are blocked by an aperture(3) creating a high contrast image at(4). Observe how scattered light with small angles are not blocked, causing some loss of contrast.

•Optical Fourier Filtering for Improved Contrast

Now consider the light field signal from above entering and propagating through a scattering medium. Scattering events in the medium will cause photons to change direction. Since the original direction of the photon is directly linked to a Fourier component, the scattering events will cause a loss in frequency information. Most of the image information is typically contained in the lower frequencies (small angles), while multiply scattered light is spread over all angles creating false high frequency information. This means that large angles have a lower ratio of real frequency information to multiply scattered light. A low pass filter, implemented by inserting a round aperture in the Fourier plane, can therefore be used to effectively filter out the false high frequencies that have been generated by the scattering events. This is illustrated in Figure 10. The low pass filtered image has a higher ratio of unscattered-to-scattered light, leading to an improved contrast. Naturally, any real high frequency information will also be lost. Thus, there is a trade-off between increasing contrast and losing some image details. Figure 11 shows a FF image next to the unfiltered image from Figure 2. The figure clearly shows the increase in contrast from Fourier filtering. The loss of high frequencies connected to the filtering manifests itself as a black ring at the center of the star, where frequencies are high.

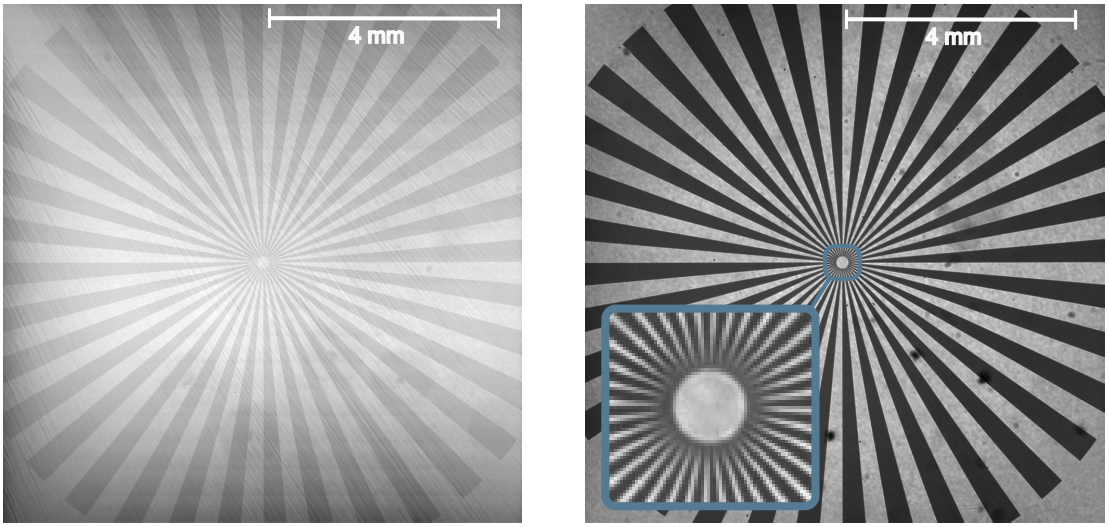

(a) Imaging through turbid water.

(b) Optically Fourier filtered image.

Figure 11: Images taken through the same scattering media without filtering and with Fourier filtering. The FF image clearly has higher contrast but also lacks some high frequencies, which can be seen in the center.

3.3 Combining Structured Illumination and Fourier filtering

As discussed above, Structured Illumination and Fourier filtering both have limitations. In SI the modulation needs to be visible and well resolved through the scattering medium. This limits the use of SI to fairly low turbidities. When the modulation structure is apparent the technique is capable of recovering high contrast without any trade-off. Fourier filtering is limited as the approach suppresses high frequency components. Although the technique works at high turbidities($10 \leq \mathrm{OD} \leq 15$), more frequencies have to be suppressed to obtain sufficiently high contrast. When combined, Fourier filtering can be used to filter enough to render the modulation visible. This allows the rest of the contrast to be regained through SI, which does not damage the high frequency information. This way, the suppressing of high frequencies is minimized while still recovering high contrast through high optical depths.

When using Fourier filtering it is ideal that the initial light source is perfectly collimated. If this is the case, all parts of the beam will be filtered equally well as all light travels along a uniform direction. If the beam is diverging, the outer parts of the beam will travel at a larger angle than the central part. When introducing any spatial frequencies to the already diverging beam, the angles connected to the frequencies(Eq.6) will be added to the divergence angles. This complicates the relationship between frequencies and angles of incident at the lens, and subsequently the aperture. Instead of a sharp cut-off frequency, the aperture creates a cut-off transition. The propagation angle of low frequencies far from the center of a diverging beam is dominated by the divergence angle. At some distance from the center of the beam the divergence angle equals the cut-off angle, beyond this radius even the fundamental frequency will be blocked. Since Fourier filtering of a divergent beam also affects frequencies lower than the cut-off, the contrast enhancing is less effective.

In order to use SI, the structure must be in-focus together with the object of interest. It is impractical to physically impose the structure right by the object, as it is presumably inside the scattering medium. Instead a one-to-one image of the modulation structure has to be formed onto the plane of the object. This imaging of the modulation causes the beam to diverge. As a diverging beam cannot be avoided, a beam diverging as little as possible is desired. This can be achieved by using a lens with a long focal length. This leads to a trade-off between the practicality and low losses of a compact setup, and low divergence. The best conditions achievable is a long focal length, yielding low divergence, and a small object as close to the beam center as possible, where divergence is low.

4 Quantifying image contrast

4.1 Modulation Transfer Function

The contrast of an image compared to the contrast of the physical object describes the performance of the imaging optics. The comparison shows how much loss of contrast the imaging optics introduces. The Modulation Transfer Function(MTF) is a standard way of describing the performance of imaging optics, as a function of spatial frequency[2, p. 579]. By including a scattering medium as part of the optics, the combined effect of the optics and the scattering medium is measured. Calculating the MTF for different optics, such as the FF and SI setups above, through the same scattering medium enables an objective comparison of the performances of the two filtering techniques.

In order to calculate the MTF value of an imaging system for a single frequency, a striped pattern of black and white linepairs with that frequency is imaged. The contrast of the image is then compared to that of the imaged pattern. The Michelson contrast(M_f) for such a pattern is defined as

$$M_f = \frac{I_{max} - I_{min}}{I_{max} + I_{min}}, \tag{7}$$

where I_{max} is the intensity of the white lines and I_{min} is the intensity of the black lines. Eq.7 will give a high value if the intensity difference between the black and white is large compared to the average intensity, thus describing contrast. The MTF value then compares the Michelson contrast of the image with that of the imaged object. The MTF value at each frequency is defined as

$$MTF_f = \frac{M'_f}{M_f}, \tag{8}$$

where M'_f is the contrast value of the image while M_f is the true contrast value of the physical object[10]. In the case of a perfect black and white pattern, M_f=1 and the MTF value equals M'_f. In the trans-illumination detection mode this corresponds to a pattern that totally blocks and totally transmits, such as the sector star used in this project. The sector star is practical since it contains a range of spatial frequencies and therefore enables measurement of the full MTF from a single image. Around the outer part of the sector star the frequency is low, and near the center the frequency is

high. The frequency of the sectors decrease as one over the radius when moving from the center toward the edges. This is illustrated in Figure 12. The conventional striped charts used to calculate MTF only give a single discrete frequency value from each black and white pattern.

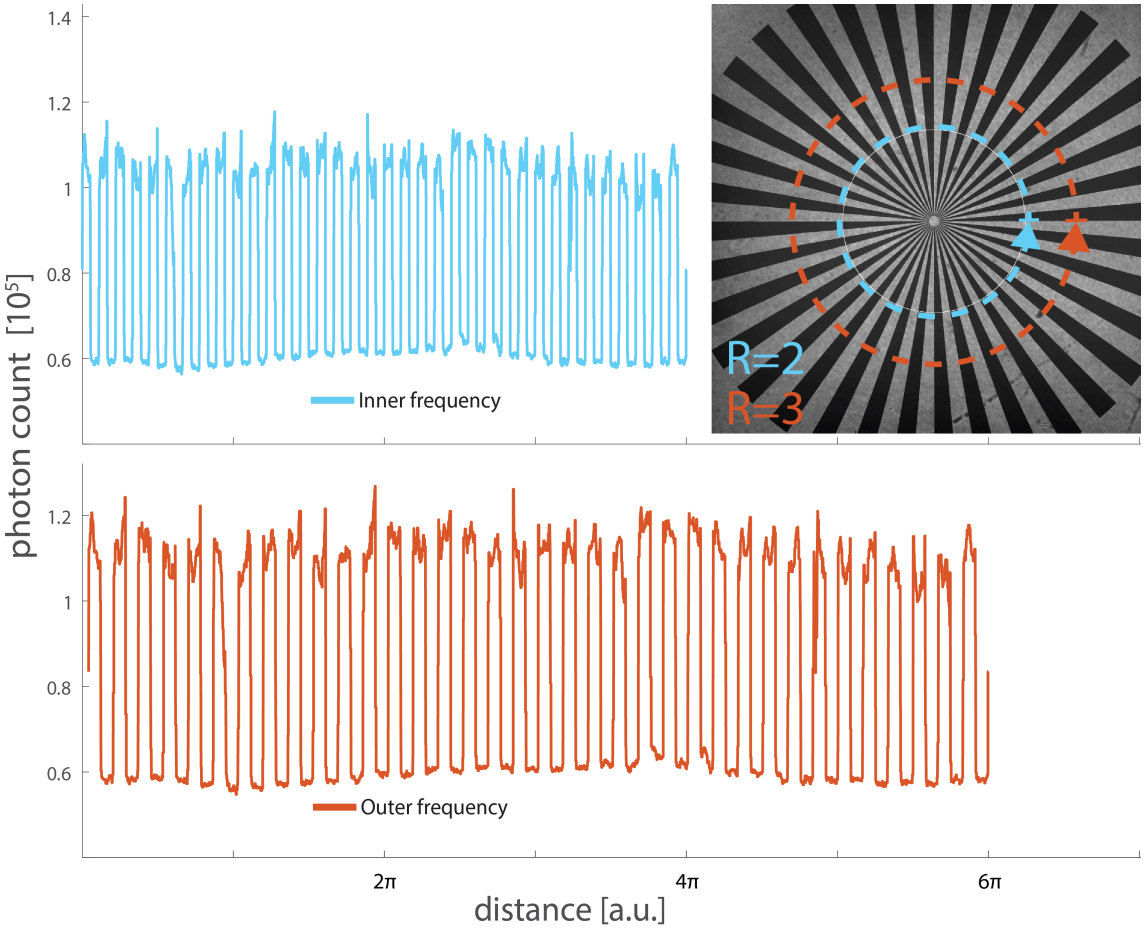

Figure 12: The blue and red dashed circles have radius's corresponding to the two frequencies to the left. The sector star has 36 sector pairs and the circumferences of the circles are 4π and 6π, giving frequencies of $9/\pi$ and $6/\pi$ respectively.

4.2 Calculating the MTF from the Fourier domain

An alternative approach to calculating the MTF_f is to use the Fourier transform(FT) and compare the strengths of the zero-order to that of the first order of a periodic modulation. The intensity of a sinusoidal modulation pattern can be expressed as

$$I(x) = I_0 + I_f sin(2\pi x f_{mod}), \tag{9}$$

where f_{mod} is the frequency of the linepair pattern. Using this example it can be seen that the average intensity is $I_0 = (I_{max} + I_{min})/2$ and the modulation amplitude is $I_f = (I_{max} - I_{min})/2$. By comparing with Eq.7 we see that $M_f = I_f/I_0$, where I_0 and I_f can be identified in a Fourier expansion ($\mathcal{F}(f)$) of the imaged pattern. In the sinusoidal case, I_0 equals the absolute amplitude $|\mathcal{F}(0)|$ while I_f is $2|\mathcal{F}(f_{mod})|$. Likewise, for a square modulation the amplitudes can be identified as $I_0 = 2|\mathcal{F}(0)|$ and $I_f = \pi|\mathcal{F}(f_{mod})|$ [10]. The Michelson contrast of a square modulation is therefore

$$M_f^{square} = \frac{\pi|\mathcal{F}(f_{mod})|}{2|\mathcal{F}(0)|}. \tag{10}$$

The benefit of using Eq.10 over the direct definition in Eq.7 is that it is applied to the full linepair pattern at once. This makes the approach more robust against noise. Simply taking the maximum and minimum value of a noisy signal and apply Eq.7 results in an overestimation of the M_f value. These values will be respectively higher and lower than the true maximum and minimum of the noiseless signal. To avoid this, an average of several samples should be used for the values of the maximas and minimas, as well as an average M_f over several periods of the linepair pattern.

5 Image post-processing and MTF calculations

The first part of this section describes the post-processing scheme used to suppress residual lines in SI and SIF images. The second part describes a Matlab code for calculating the MTF from an image of the sector star, specifically developed as part of this project. The third part compares two different versions of the MTF code. The fourth part discusses the calculated MTF:s of an example of FF and SI imaging through turbid water. The fifth part investigates the effect of residual lines suppression on the MTF.

5.1 Residual lines suppression in structured illumination

In theory, the three modulated sub-images recorded when using structured illumination can perfectly create the full image. In practice however, this is never the case. Small variations in intensity between the three images or a less-than-perfect imaging system are examples of disturbances that causes the combined image to suffer from structure artifacts. This appears as visible line structures on the image, typically at higher orders of the modulation frequency.

To suppress the lines the images have to be post-processed(p-p). The post-processing scheme for suppression of residual lines in structured illumination described in this section was developed in Matlab. The scheme is performed by the following steps:

- The combined structured illumination image is Fourier transformed
- The residual frequencies are located
- A mask blocking those frequencies is created, where each blocked area is defined by a Gaussian shape
- The mask is applied to the Fourier transform of the image
- The transform of the image is inverse Fourier transformed to obtain a post-processed image without residuals

The residual frequencies are be located by finding peaks along the axis containing the modulation frequency in the Fourier transform, e.g. the y-axis for a vertical modulation. The mask altering the amplitude at these frequencies is constructed by creating Gaussian shaped holes in a matrix of ones. The mask is then applied by multiplying it to the variation from the mean value of the the Fourier transformed image. By using Gaussian shaped areas which do not introduce sharp edges in the Fourier transform, the introduction of new frequencies is avoided. However, blocking spacial frequencies inevitably reduces the contrast of the image. It is therefore desirable to block as little as possible while still suppressing the artifacts sufficiently. Unfortunately, the modulation, and by extension the artifacts, can't be at a too high frequency for SI to work satisfactory. In this project a modulation of 5 linepairs/mm is used on a system that resolves up to around 50 linepairs/mm. This means that the post-processed image might suffer reduced contrast in the modulation direction at

5, 10, 15 linepairs/mm etc. If the artifacts are at too low frequencies it is not possible to filter them out without damaging the main information of the image. The post-processing scheme is illustrated in Figure 13.

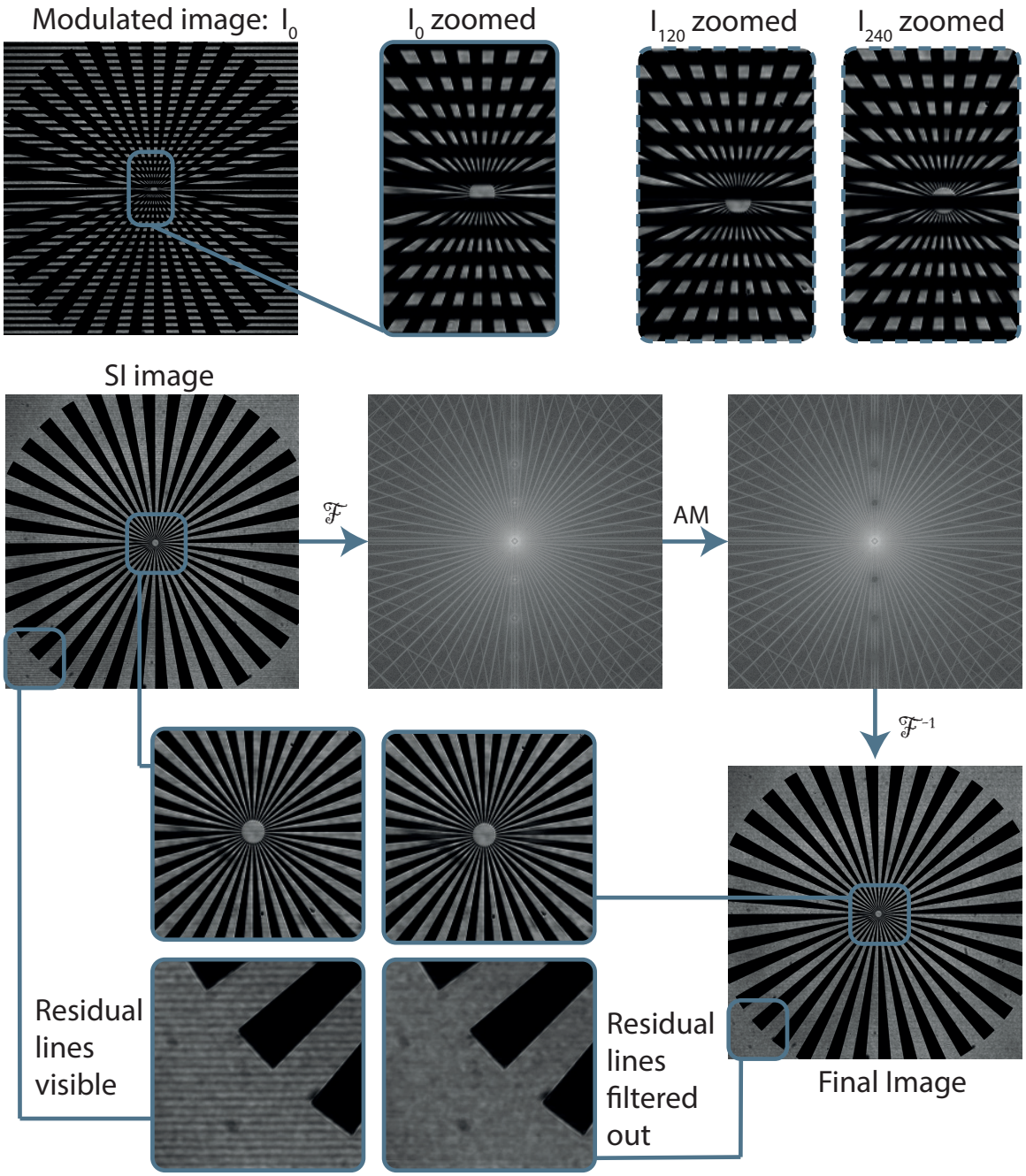

Figure 13: Illustration of the post-processing scheme. The three phase-shifted modulated images are combined to one full image using Eq.5(SI image). The combined image is Fourier transformed($\mathcal{F}$) using fft2 in Matlab and multiplied with an amplitude mask(AM). The final post-processed image is then obtained by taking the inverse Fourier transform($\mathcal{F}^{-1}$). The final image has less residual lines but suffer from reduced contrast at the blocked vertical frequencies.

5.2 Description of the MTF Matlab code

As part of this project a Matlab code was developed specifically to calculate the MTF of an optical system from an image of the sector star target. The code samples circles of increasing radius around the center of the star, producing a one-dimensional square pattern for each sampled radius. In order to sample equidistant frequencies, more circles are sampled close to the center, since the frequency is proportional to one over the radius. An example of a sampled frequency in a high and low contrast image is shown in Figure 14.

The code exists in two versions:

•The definition version implements the MTF calculation by the definition in Eq.7. The peaks of the sampled square pattern are found by finding the maximum cross-correlation to a generated square pattern. A user defined number of points are then sampled around each minimum and maximum and used to calculate the average M_f using Eq.7.

•The Fourier Transform version calculates the amplitudes of the fundamental and first order frequencies by calculating the Fourier transform of the sampled square pattern. From this the M_f, and subsequently the MTF, can be calculated by implementing Eq.10.

By default, both versions samples 360° around the star to calculate the average MTF. But the codes also allows for the user to specify a sector on which to perform the calculation, making it possible to calculate the MTF of e.g horizontal and vertical frequencies separately.

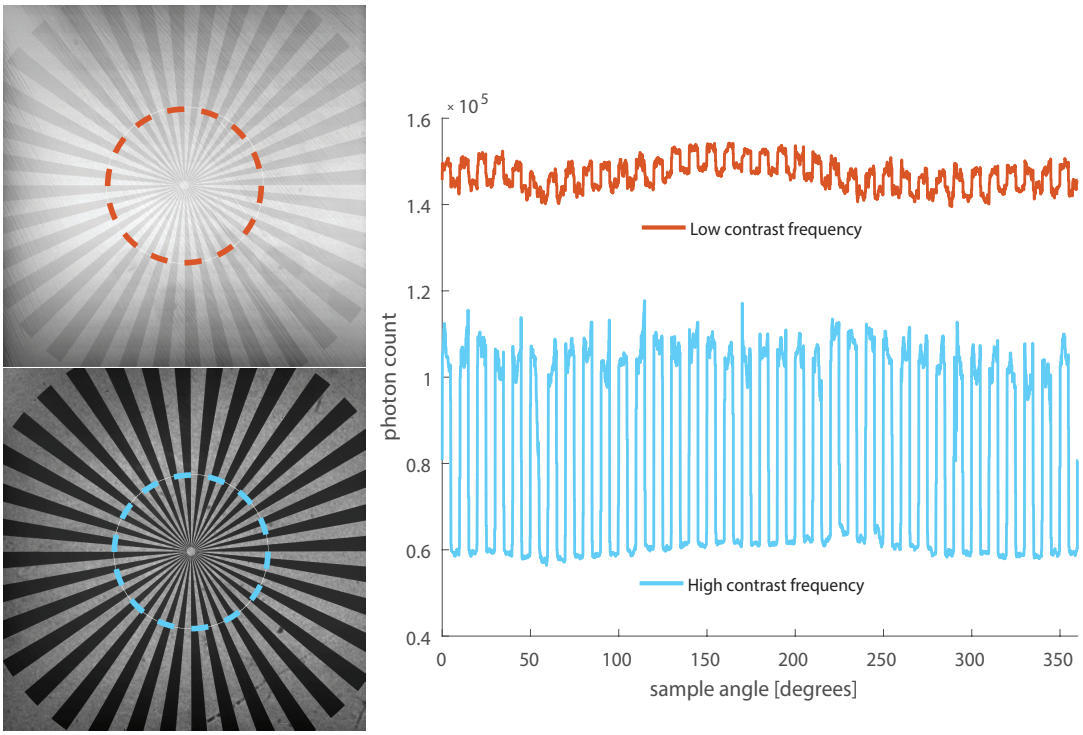

Figure 14: An illustration of the MTF code's sampling of a single spatial frequency from the sector star. The same frequency is sampled in a low contrast image(top) and a high contrast image(bottom). The sampled rings creates the one dimensional frequencies(right). The low contrast frequency(red line) has a much lower amplitude and a higher average intensity, than the high contrast frequency(blue line).

As any calculation from sample data, the MTF calculations suffer from sampling noise due to the discrete number of pixels that form the image. Sampling in circles also introduces more sampling noise than sampling along a straight line. The circles themselves are defined with float precision from a center and the code picks the values of the pixels that the circle passes through. This means that the circle is represented by values of pixels whose distance to the center is not the exact radius, but rather varies by $\sqrt{2}$ times the pixel size. The net result of the sampling errors is an MTF curve with a high frequency noise. The noise can be suppressed by averaging over adjacent frequencies, by using a wider circle, or over different sampling along the same circle.

For the calculation to produce the correct MTF values it is crucial that the exact center of the star is found. If a circle is sampled while being off-center, the one-dimensional square pattern will not contain a single frequency square pattern, but rather an oscillating frequency. For this reason, a centering calculation is performed in the code before the complete MTF calculation can be performed. The centering code uses the same MTF calculation as the MTF code itself, but at fewer frequencies. It assumes that the center of the star is where the mean value of the MTF for those frequencies is at its highest. The centering needs to be performed with sub-pixel precision due to the sensitivity of the MTF calculation. Figure 15 shows how the mean MTF value varies as the center is moved around the real center of the star. The speed of the optimization algorithm scales with the area of the image. In order to avoid searching over the full image, the user is asked to define an area of the image which definitely includes the center. For high resolution images or images with very low visibility, i.e. large uncertainty in the center location, the centering algorithm takes most of the computational power required by the code.

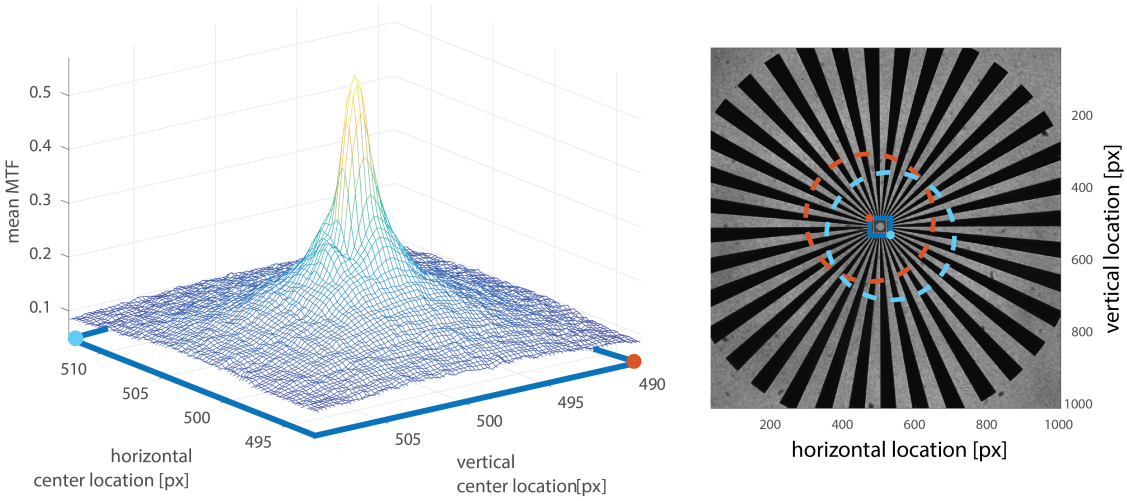

Figure 15: The peak to the left shows how the mean MTF varies when moving the center location in the area specified by the blue square in the center of the sector star to the right. The red and blue dots show two examples of center locations and their corresponding location in left figure. The narrowness of the peak demonstrates the high sensitivity of the MTF to center location.

5.3 MTF calculation comparison

Having implemented two approaches for the MTF calculation, using Eq.7 and Eq.10 respectively, they can be compared to see if both implementations produce the same MTF. The MTF calculated by the definition is denoted MTF_{def} and the MTF calculated by Fourier transform is denoted MTF_{FT}. Figure 16 shows the MTF for imaging through clean water with and without FF, calculated with both implementations.

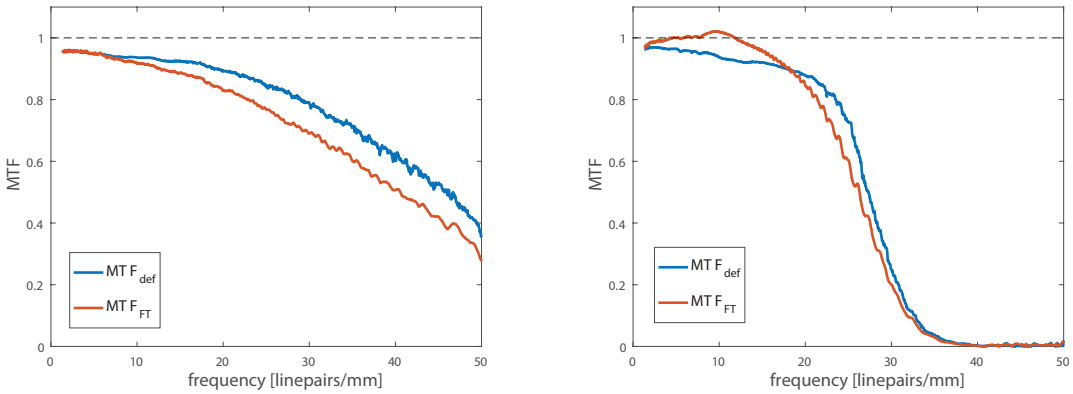

(a) (b)

Figure 16: Comparison between MTF calculation using the definition given in Eq.7 and the Fourier transform approach from Eq.10. The graph to the left shows the MTF:s for unfiltered imaging. The graph to the right shows the MTF:s for FF imaging. Notice how the MTF_{FT} increases with frequency and surpasses unity in the FF case.

Surprisingly, Figure 16 shows that the two implementations do not produce identical results. The MTF_{def} and MTF_{FT} of the unfiltered imaging are identical at low frequencies but differs at higher frequencies. For the optical Fourier filter imaging, MTF_{def} and MTF_{FT} differ even more. The MTF_{FT} increases with frequency in the low frequency domain, which is an unexpected behaviour. The contrast is typically lower at higher frequencies. Furthermore, MTF_{FT} not only approaches unity, but actually surpasses it, which is impossible with the MTF definition. Considering both the unexpected behaviour and the higher than unity values, the MTF_{FT} code appears to be less reliable. Probably, the optical Fourier filtering changes the shape of the star pattern in such a way that the MTF_{FT} derivation is no longer valid. It is possible that the underestimation of the MTF_{FT} implementation at higher frequencies originates from a similar problem. It could also be an overestimation of the MTF_{def} implementation due to noise from insufficient sampling. Whichever the case, this comparison shows that the two implementations are not interchangeable. For consistent results all MTF calculations in this project will therefore be performed using the MTF_{def} implementation.

5.4 MTF of FF and SI for an Example of Turbid Water

With the MTF code as a tool it is possible to properly quantify contrast improvement. The MTF:s for clean water, turbid water, FF, and SI imaging in Figures 8 and 11 are plotted in Figure 17.

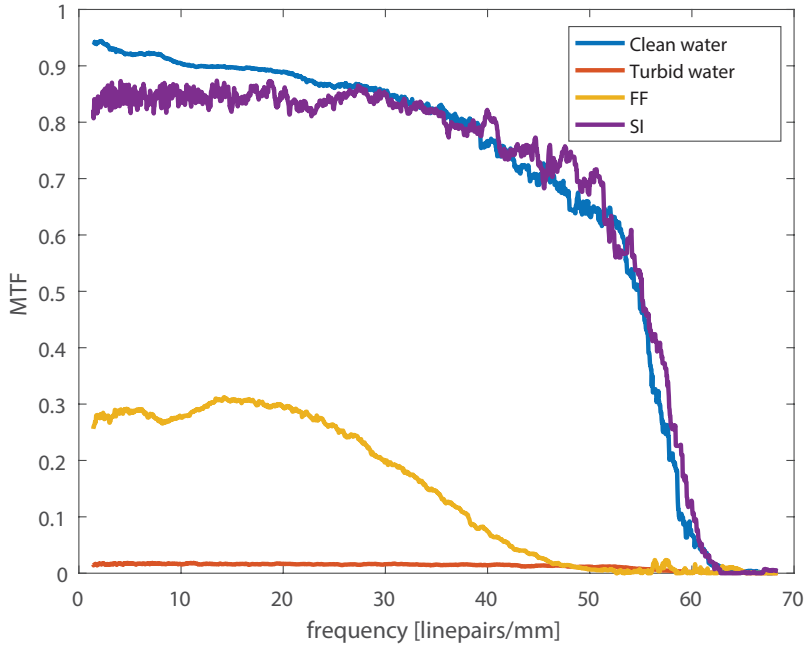

Figure 17: The MTF:s of the clean water, turbid water, FF and SI example imaging in Figures 2, 8, and 11.

From these results strengths and weaknesses of the filtering techniques can be identified. The contrast of the through the turbid water is very low. The Fourier filtering improves the contrast by 10 times from the unfiltered case at low frequencies, but then loses all contrast above the cut-off frequency at 30-35 linepairs/mm. The SI filtering improves the contrast by 30 times across the entire spectral range. The contrast in the SI image is even comparable to the image with no scattering medium at all. Between 50-60 linepairs/mm even the image through clean water looses all contrast. That is the limit of resolution of the camera. Since the capabilities of the camera is not of interest in this project, all other MTF:s are only presented up to 50 linepairs/mm.

5.5 Effect of residual lines suppression on the MTF

The MTF code enables a closer look at how the residual lines suppression influences the contrast. In Figure 18, the MTF from a post-processed SI image is presented together with the MTF from the unprocessed image. To emphasize its effect on the MTF, the size of the blocking mask have been slightly exaggerated. The MTF from the post-processed image is presented for horizontal and vertical frequencies individually, as well as the average MTF. Using the sector star it is not possible to truly sample horizontal and vertical frequencies. Instead, the star is divided into sectors considered either horizontal or vertical. Since there is less data available, the partial MTF:s are more noisy. Figure 18 include the sampling of horizontal frequencies.

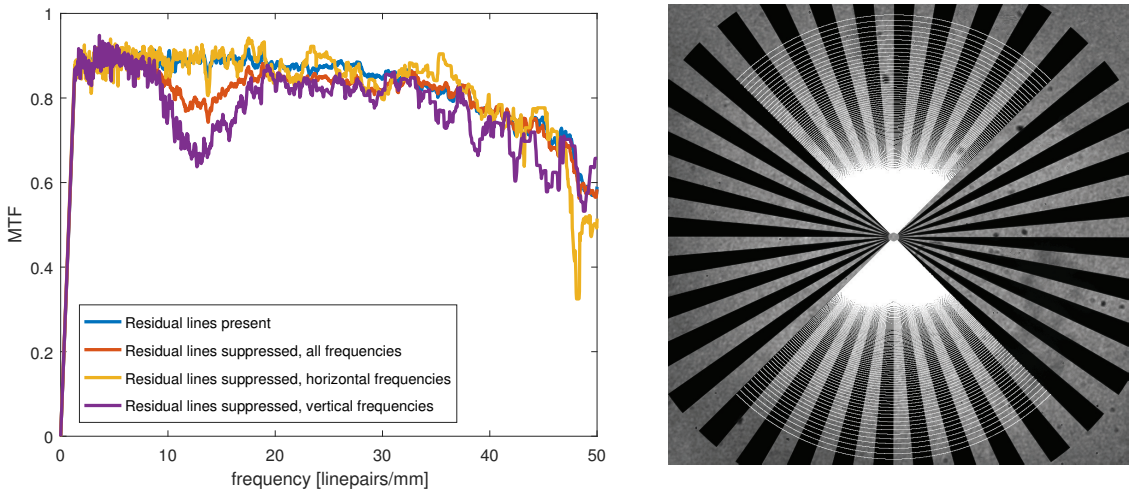

Figure 18: Example of the effect of residual lines suppression on the MTF. The modulation frequency is 5 linepairs/mm. A large decrease in contrast is seen at 3 times the modulation frequency, as well as a small dip around 3 linepairs/mm. To the right is the sampling of the code to get horizontal frequencies.

The figure shows a substantial decrease in contrast at 15 linepair/mm for the vertical frequencies, while horizontal frequencies are largely untouched. A smaller decrease appear at around 3 linepairs/mm indicating that residual lines suppression affect contrast at other frequencies than that of the residual lines. It is clear that the negative impact on the contrast from the post-processing can be severe. Post-processing must therefore be applied with care. By adjusting the shape and size of the blocking mask it is possible minimize the impact on the image contrast when suppressing the artifacts sufficiently. In some cases, visible artifact lines might be preferred over loss of contrast.

6 Experimental setup

The first part of this section provides a description of the optical SIF setup that has been developed and used in this project. The second part describes the probed scattering medium. The last part describes what measurements were made using the setup.

6.1 Description of the optical setup

Figure 19 shows the final optical setup developed and used during this project. The setup consists of three built-in solid state lasers(1) of 473 nm, 532 nm and 671 nm wavelength. The beams are focused by a spherical plano-convex lens(2) through a speckle-reducer(3) and into 1 mm diameter optical fiber(4). Exiting the fiber the light is collimated by a spherical bi-convex lens(5) of focal length 100 mm. The collimated beam have a diameter of D=1.8 cm. A Ronchi grating mounted on a piezo micro-traverse(6), which can be moved in and out of the beam-line, imposes a modulation structure onto the beam. The Ronchi grating is 25×25 mm and has the frequency 5 linepairs/mm. A spherical bi-convex lens(8) of 1 m focal length is used to form an image of the grating onto the object of interest, a 10 mm in diameter sector star target(9). As a one-to-one image is formed, a 4 m long distance is required. To keep the dimension of the optical setup reasonable, a series of mirrors(7) have been used. The beam illuminates one of the three cubic cuvettes(10) of 2 cm, 3 cm and 4 cm, containing a scattering dispersion of polystyrene micro-spheres in water. The transmitted beam is split into two paths by a 50-50 beam-splitter(11). The beams are collected by two different

objective systems and imaged onto two identical CCD cameras. The first objective system is a telecentric objective(14) and the second is a regular objective with an adjustable aperture at its focal plane(15). The cameras have a maximum intensity resolution of 14 bit.

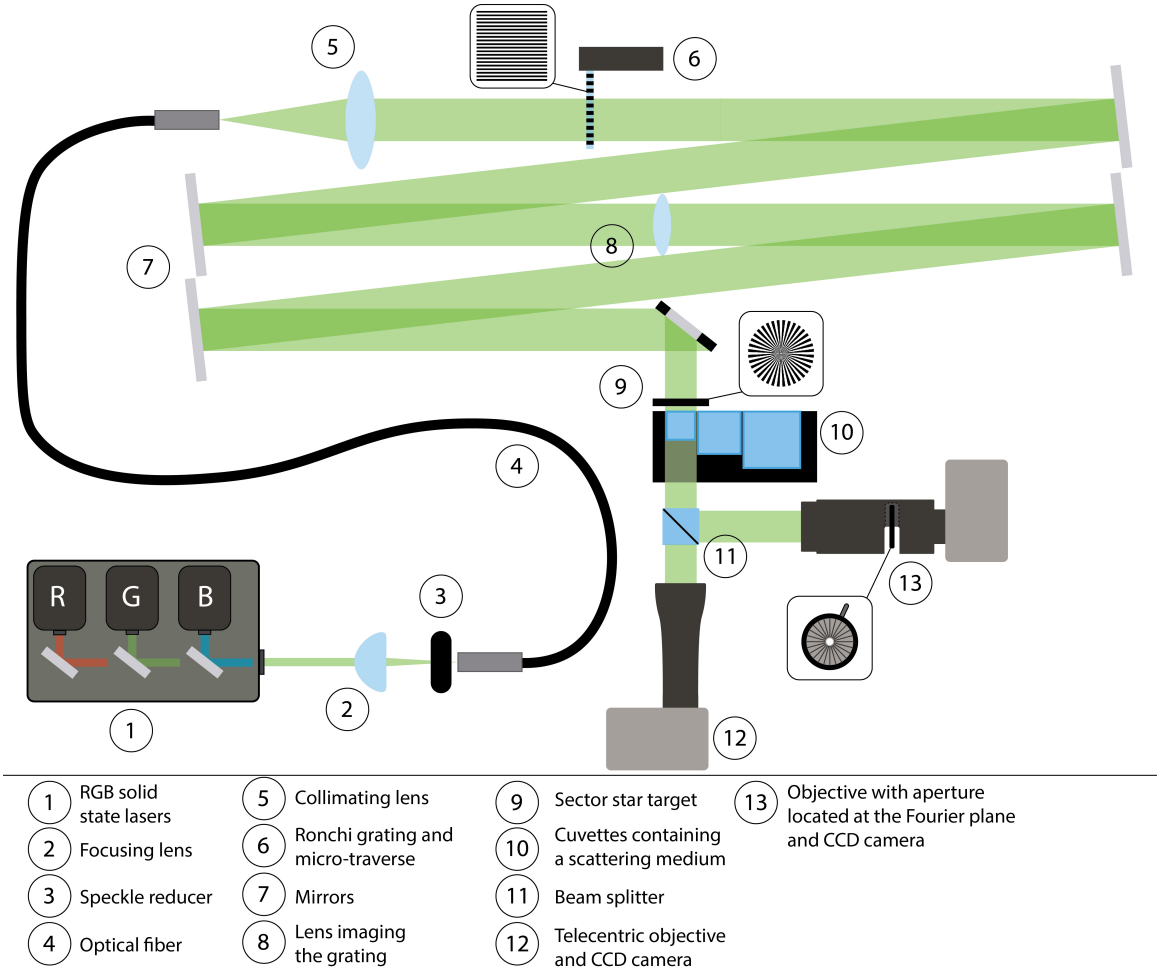

Figure 19: The imaging setup developed and used in the project. The beam path between the Ronchi grating and the sector star is 4 m. Two different Fourier filtering camera systems are used in parallel.

During the course of the project the optical setup went through multiple changes. The first design was a replica of the setup used in the proof-of-concept article on SIF[10]. This initial setup did not include the lens imaging the modulation onto the sector star. Instead, the modulation grating was placed right next to the sector star ensuring that they could both be imaged simultaneously. The lens was added in this project to make the SIF concept more practical in real applications. The imaging lens in the final setup has a focal length of 1 m, this means that the full length of the one-to-one imaging is 4 m. The focal length is chosen to be long in response to the need for FF to use a beam as collimated as possible, as explained in subsection 3.3. A long focal length ensures that the beam has as small divergence as possible. An earlier iteration of the setup used a 30 cm focal length. That setup showed traces of the predicted issues with a diverging beam. The 1 m lens proved to limit those issues sufficiently. A photograph of the final setup is shown in Figure 20.

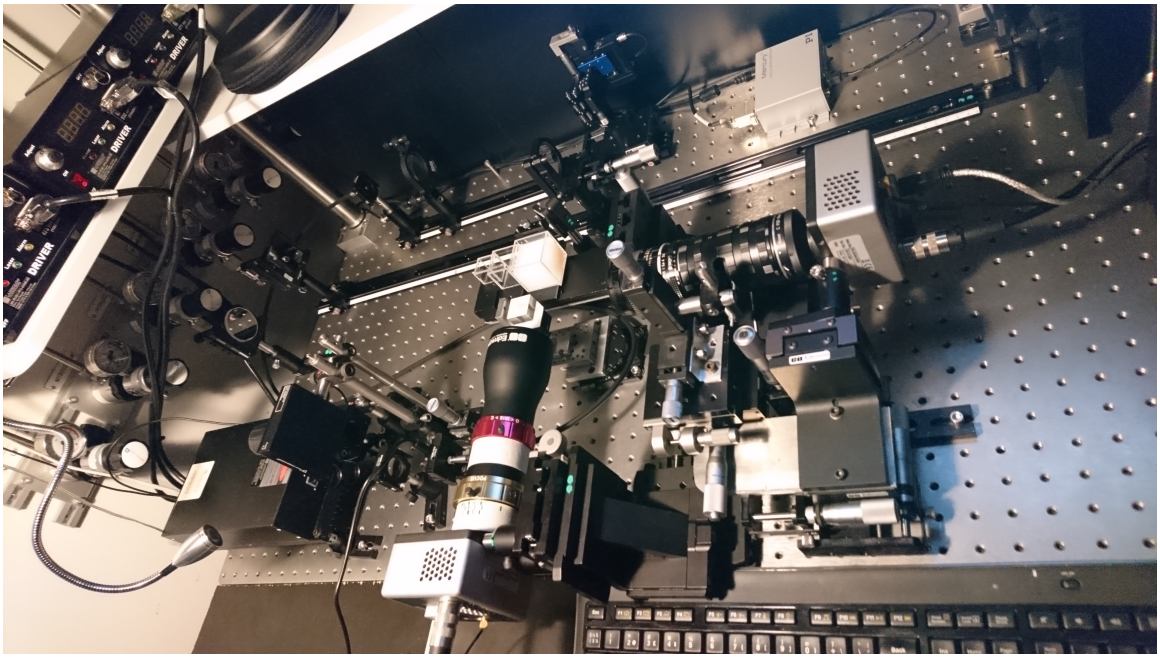

Figure 20: A photograph of the final setup.

The effect of divergence on Fourier filtering is of even more importance when using the sector star to represent different frequencies. As the sector star is placed in the center of the beam, it connects frequencies to locations in the beam. The center of the star holds the high frequencies and is in the center of the beam, where the divergence is smallest. The Fourier filtering will therefore affect the MTF at high and low frequencies differently. This will make the cut-off frequency less distinct and more of a transition.

Other components were added to improve the setup. These include the optical fiber and the speckle reducer, which both serve to obtain a homogeneous beam profile. Most components in the final setup are mounted in a way that they can easily be adjusted. These include the two cameras, which are adjustable in 3D, the imaging lens and the Ronchi grating. To also be able to switch between FF, SI and SIF, the Ronchi grating and the imaging lens can easily be flipped in and out of the beam line and the aperture opening adjusted. The final setup shown in Figure 19 includes all of this functionality and still remains very compact. The full setup is mounted on an optical table of 1 $\times$ 0.8 m.

A telecentric lens is an optical system designed to have a zero angle field of view. This is a feature commonly used in machine vision when the perception of depth hinders accurate measuring[14]. As discussed in section 3.2, incoming angles are related to Fourier components. This means that a telecentric lens effectively does similar things as the Fourier filtering setup in Figure 9. The telecentric lens has been included in the optical setup in order to investigate if a telecentric lens is suitable as a Fourier filtering tool for SIF. All Fourier filtering in this project is therefore performed both with a custom aperture setup and with a telecentric lens. The used telecentric lens has an adjustable iris, which allows its Fourier filtering capability to be turned on and off.

6.2 Description of the measurements

The scattering medium used in this project is a single dilution of polystyrene spheres in filtered water. The spheres have diameters D = 0.13 µm and refractive index of $n_p^{473} = 1.587 - 0.0004i$, $n_p^{532} = 1.584 - 0.0004i$ and $n_p^{671} = 1.5805 - 0.0004i$ for blue, green and red respectively[15]. The known optical properties make it possible to create a controlled scattering medium for the experiments, as well as accurately simulate the medium. The online multi-scattering software[1] was used to calculate the particle number density required to obtain OD = 7.5 for the blue illumination($\lambda = 473$ nm) through 2 cm of dilution. The dilution mixture could then be derived to obtain the desired OD. The OD for the other wavelengths could then be calculated from the known particle number density(and optical properties), again using the software. Figure 21 shows one of the cuvettes filled with the scattering medium illuminated by the blue, green and red laser. Observe the glow from the highly isotropic scattering. In Figure 20 the same cuvette is included in the full setup. In white room lighting the scattering dilution is white.

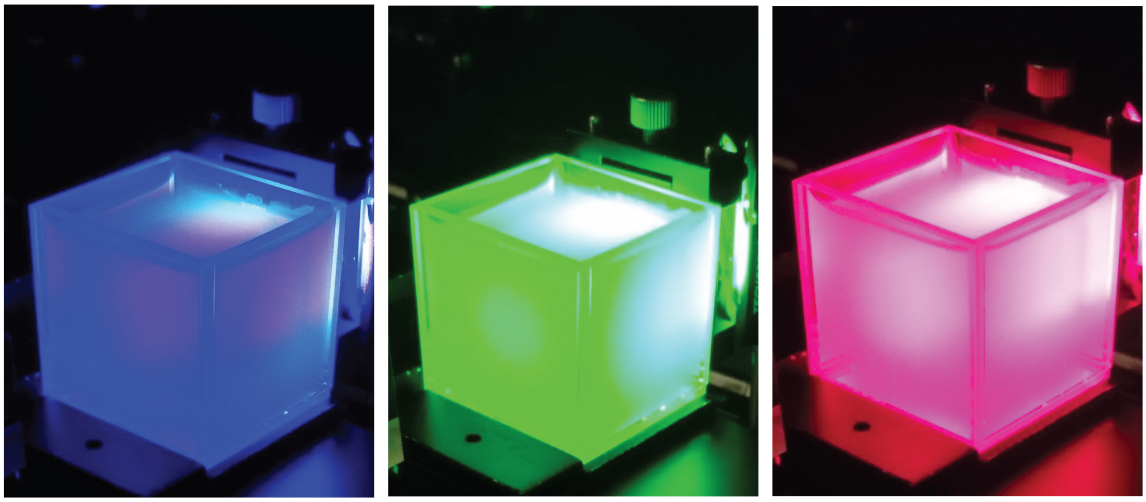

Figure 21: Photographs of a cuvette filled with the scattering dilution illuminated by the blue, green and red laser.

The experiments investigate how FF, SI and SIF are affected by two main factors: the optical depth of the scattering medium and the illumination wavelength. The performance of SIF is then compared to the other two. To do this, measurements are made for 9 combinations of three cuvette sizes and three wavelengths. A single dilution is used and the size of the cuvette makes the optical depth vary. The optical depth also varies between the wavelengths due to the chromatic dependence of the scattering cross-section(see Figures 1a and 1e). Table 1 summarizes the optical depth of each case.

	OD		
	2 cm	3 cm	4 cm
red ($\lambda = 671$ nm)	2.20	3.30	4.40
green ($\lambda = 532$ nm)	5.01	7.52	10.03
blue ($\lambda = 471$ nm)	7.50	11.25	15.00

Table 1: Optical depths of the 9 combinations of cuvette sizes and wavelengths.

The optical Fourier filtering is performed by the two objective systems. The performances of the two systems, a regular objective with an aperture in the Fourier plane and a telecentric lens, are compared against each-other. The regular lens is set to an aperture opening of 3 mm in diameter for all detection cases using Fourier filtering. The telecentric lens is set in order to obtain the same cut-off frequency as the regular objective.

For each imaging case, the laser power of the illumination is adjusted such that the dynamic range of the cameras was fully optimized. This means that the incident illumination power is higher when imaging at higher optical depths and when using Fourier filtering, as less of the output light reaches the camera sensors. Thus, the maximum recorded light intensity remains the same for all images. Each image is an accumulation of 10 recordings with 0.1 s exposure time each.

7 Experimental results and discussion

In the first part of this section, results of measurements with varying OD are presented and discussed. In the second part measurement results with different wavelengths are treated.

7.1 Effect of optical depth

In Figure 22 the unfiltered, FF, SI and SIF images taken using blue light with the telecentric lens are shown. The figure provides an overview of how the different filtering methods perform at OD:s from 7.5 to 15. Visibility without filtering goes from good to non-existent in this range of OD. The third row shows that SI provides very high contrast while some visibility remains, but stops working when the modulation falls into the noise level. The second row shows that FF improves contrast at any OD case. Contrary to SI however, the FF images lose contrast continuously. The fourth row shows that SIF, like SI, provides an excellent contrast in the first two columns. At the highest optical depth, SIF provides relatively high contrast compared to SI and FF. However the SIF image is very noisy. When recording the images in the third column of Figure 22, the imaging was restricted by the maximum power of the laser. The used laser was not powerful enough to use the full dynamic range of the cameras. This causes the images to be more noisy than otherwise would have been the case.

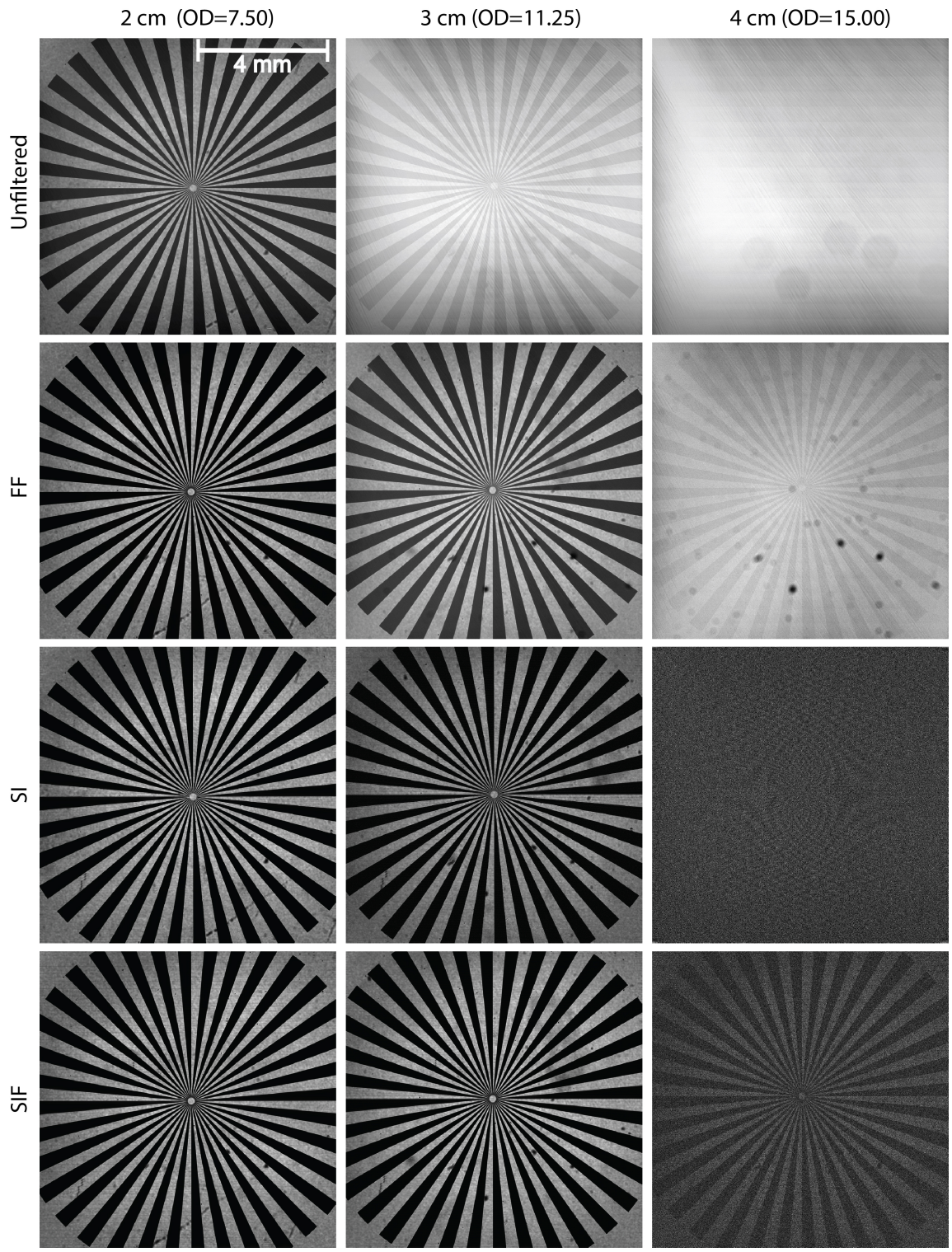

Figure 22: Sector star images showing the contrast evolution between different filtering techniques and optical depths(cuvette sizes). In the third column, the 4 cm cuvette, the differences between the results from each technique are most apparent.

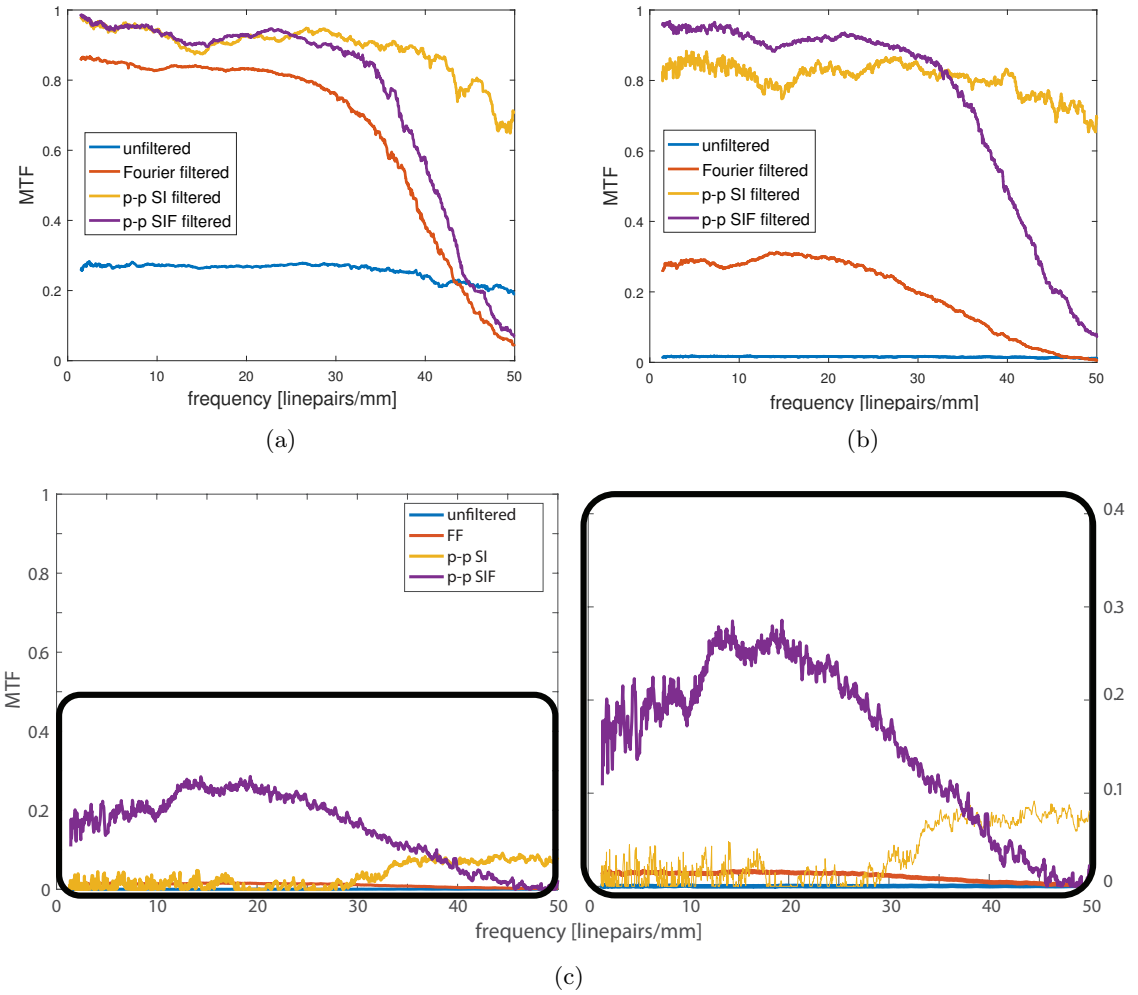

Figure 23: MTF:s from the images given in Figure 22. The three Figures (a), (b) and (c) show the MTF:s in columns 1, 2 and 3 respectively. In Figure (c), the MTF of SI imaging is mostly noise and might be considered as 0.

In Figures 23a, 23b and 23c the MTF:s calculated from the images in column one, two and three are respectively plotted. The MTF:s verify what was observed in the images. SI and SIF both provide very high contrast in the two lower optical densities and FF improve contrast but only by a certain amount. This follows the predictions of the theory, as SI and SIF should indeed be able to filter out all out-of-focus light while FF only filters out high frequency noise. But the MTF curves give a much more detailed view of the contrast than the images. Figure 23b shows that SI loses 10% contrast between OD = 7.5 and OD = 11.25, while SIF does not. Figure 23c shows that, at OD = 15, SIF provides a much higher contrast than FF. SIF provides close to 30% contrast while FF provides around 3%. It is likely that the performance of SIF would improve further with more available signal.

Figure 24 summarizes of how much FF, SI and SIF improves the contrast as a function of optical depth. The curves are calculated by taking the average MTF value from zero to the cut-off frequency and normalizing with the unfiltered average MTF. In order to have as much data as possible, all different optical depths have been used(see Table 1), regardless of illumination wavelength.

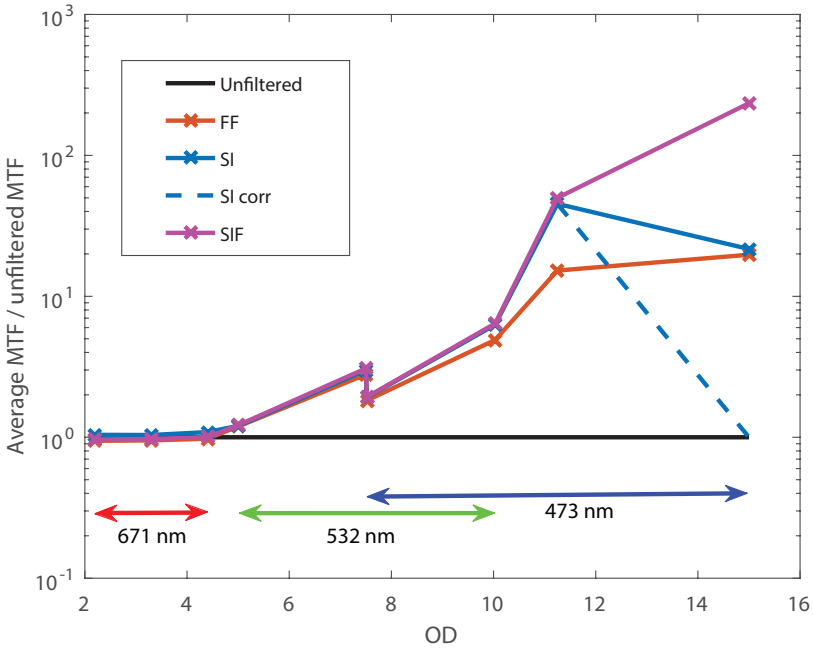

Figure 24: An overview of the contrast enhancement by FF, SI and SIF from the unfiltered case as a function of optical depth. At low OD:s they perform similarly. At medium OD:s SI and SIF outperform FF. At high OD:s SIF is superior. The dashed line is a correction of the performance of SI since the calculated value is dominated by noise(see Figure 23c). The color coded arrows show what range of OD:s is measured by what wavelength.

At low optical depths($0 < \text{OD} \leq 5$) there is little contrast to be gained from filtering so FF, SI and SIF perform equally well. At medium OD:s($5 < \text{OD} \leq 10$), SI and SIF outperform FF. As illustrated in Figure 10, a portion of the scattered light is accepted through the aperture, causing FF to continously lose contrast. For SI(and SIF) however, Figure 7 shows that very few scattering events are needed for the modulation to disappear. Almost all scattered light can therefore be filtered out. At high optical depths($10 < \text{OD} \leq 15$) SI stops working and SIF is the superior filtering technique. Note that these observations correspond to scattering by particles which are smaller than the wavelength. For larger particles with highly forward scattering phase functions, different results can be expected.

7.2 Effect of illumination wavelength

As discussed above, illumination wavelength can have significant impact on OD and scattering phase function of a medium. An example of this is seen in Figure 25, where unfiltered images recorded through the 4 cm cuvette with all three wavelengths are shown. Blue illumination is scattered the most and gives no visibility at all, while with green and red illumination the visibility remains good. Naturally, through the smaller cuvettes the visibility is better. As a result, changing illumination wavelength is the most common way to improve contrast through a given sample.

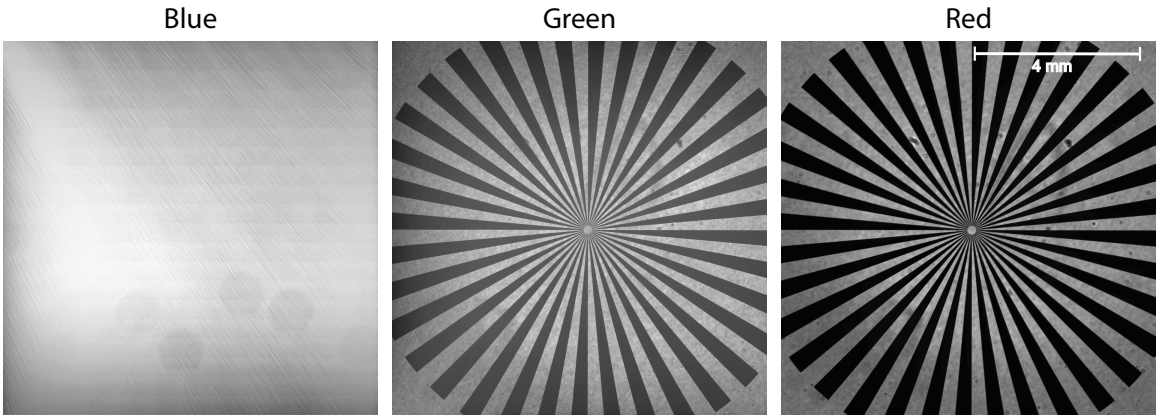

Figure 25: Unfiltered images taken through the 4 cm cuvette using blue(473 nm), green(532 nm) and red(671 nm) illumination. Blue light has been scattered the most and lost all visibility.

Figure 26 shows a comparison between SIF imaging with different wavelengths through the same medium. The figure shows unfiltered and SIF images taken through the 3 cm cuvette using the three different wavelengths: 473 nm, 532 nm and 671 nm. The optical depths of the three cases are: 11.25, 7.52 and 3.30. The visibility through the medium is largely increased when using a longer wavelength. However, while the contrast in the unfiltered images clearly varies, the SIF images look similar. In Figure 27 the MTF:s from the images are plotted.

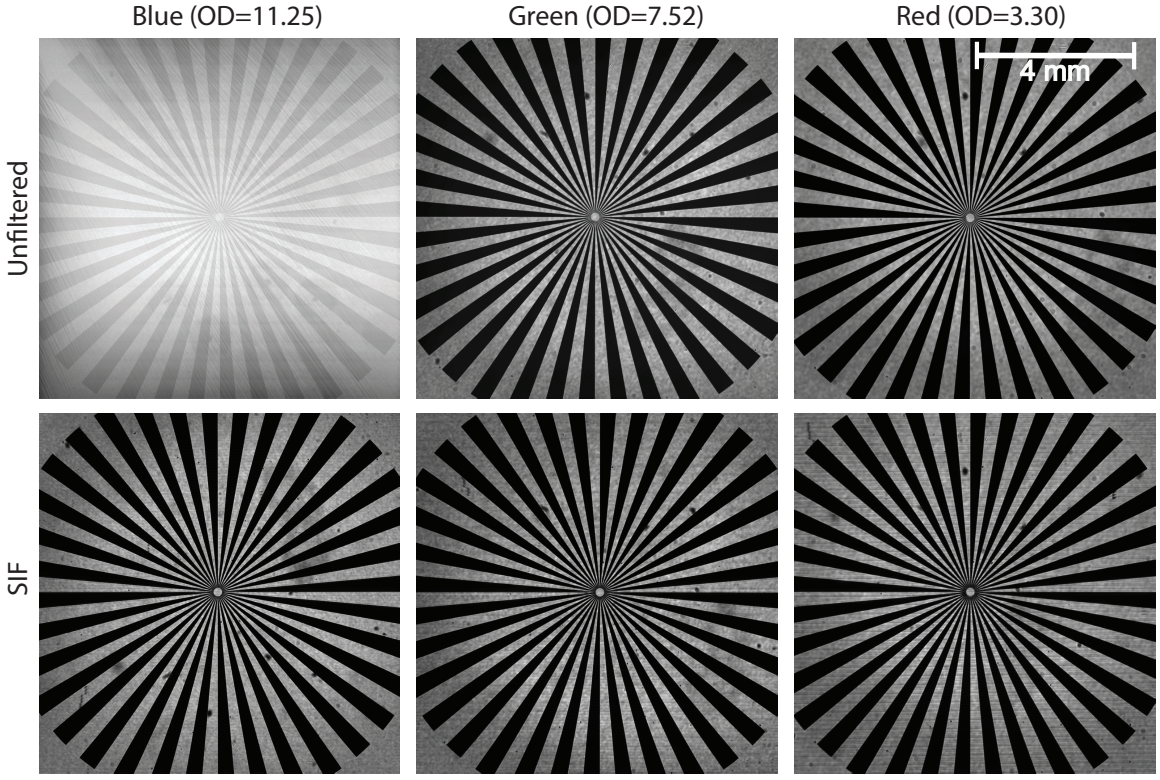

Figure 26: Unfiltered and SIF imaging through the 3 cm cuvette using blue(473 nm), green(532 nm) and red(671 nm) illumination. The contrast varies considerably in the unfiltered case but looks similar for the SIF images.

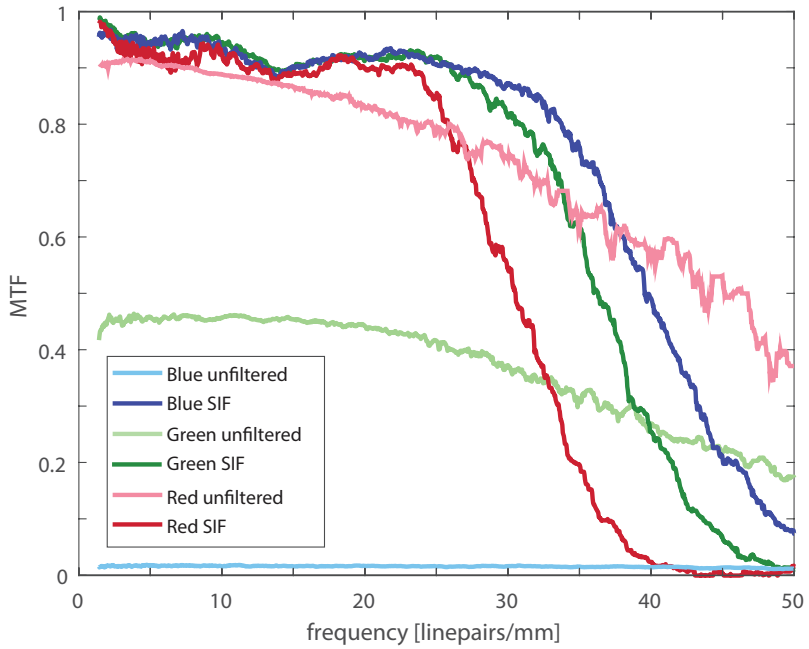

Figure 27: MTF:s of unfiltered and SIF imaging using different illumination wavelengths. The contrast varies considerably in the unfiltered case but is very similar for the SIF images.

Figure 27 shows that while the unfiltered contrast vary greatly due to the difference in OD for the three wavelengths, the SIF contrasts are almost identical, especially at low frequencies. This shows that SIF is able to compensate for the stronger scattering of lower wavelengths. This give SIF imaging a higher degree of freedom when imaging through a given sample, for example in biomedical applications. It is also noticed that the cut-off frequency is lower for the longer wavelengths. The same aperture opening has been used for all colors, so this is unsurprising considering the wavelength dependence in Eq.6. This means that the blue illumination, which scatters the most, has been Fourier filtered the least and still obtains equally high contrast.

Figure 28 shows a comparison between SIF imaging with different wavelengths through the same optical depth. The figure shows unfiltered and SIF images taken with blue light through OD = 7.5 and with green light through OD = 7.52. As explained in section 2, the scattering phase function at these two wavelengths are slightly different. The green light scatter more isotropic than the blue. The zoomed SIF images again show that the Fourier filtering cut-off frequency is lower using green light than blue.

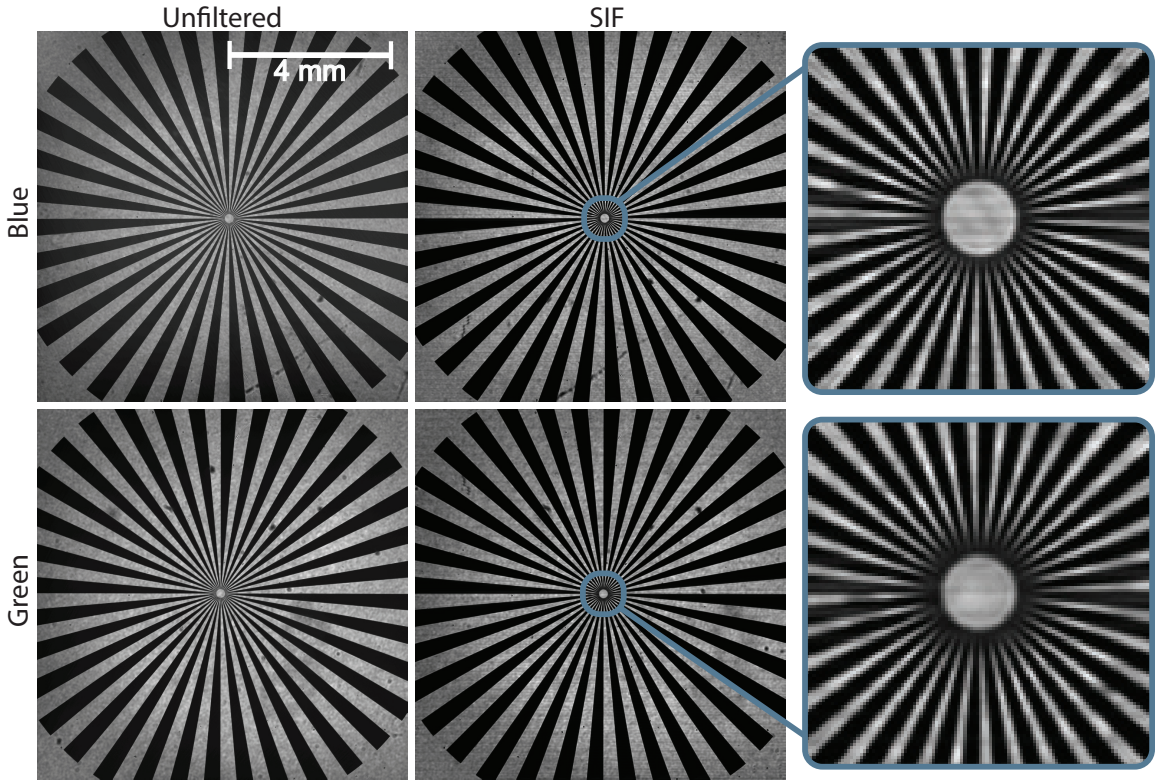

Figure 28: Images taken using blue(473 nm) and green(532 nm) illumination through OD = 7.5 and OD = 7.52 respectively. The zoomed area from the center of the sector star shows that the optical Fourier filtering reject more frequencies at 532 nm than at 473 nm.

Figure 29 shows the MTF:s calculated from the images in Figure 28. The figure confirms that the contrast in the SIF images are indeed very similar, except for the cut-off frequency being at a lower frequency for green illumination. The figure shows a rather large difference in contrast in the unfiltered images. This is due to the difference in scattering phase function, where a more isotropic scattering phase function provides higher contrast than a more forward scattering one.

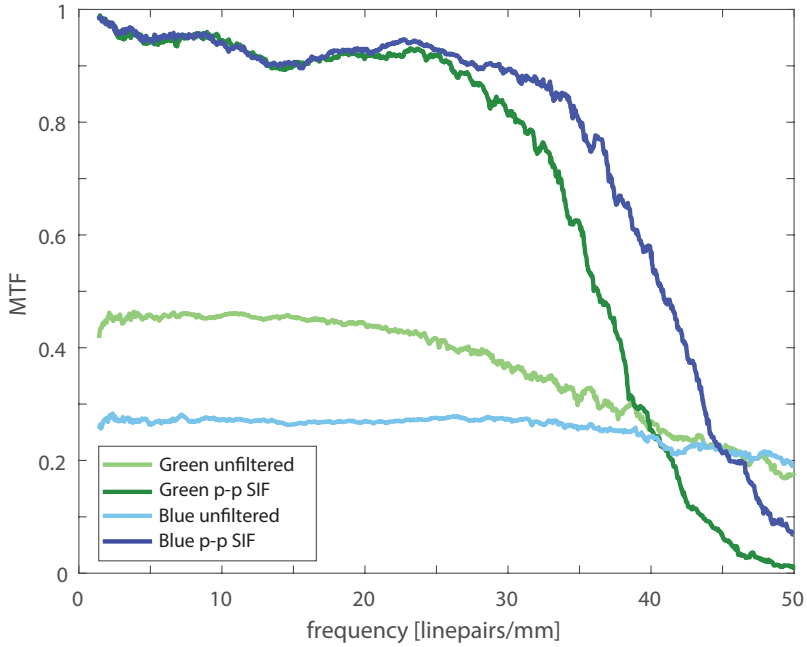

Figure 29: MTF:s of imaging using blue(473 nm) and green(532 nm) illumination through OD = 7.5 and OD = 7.52 respectively. The SIF images have almost identical contrast while the unfiltered images differ by a factor of 1.6 in the low frequencies.

7.3 Comparison between two objectives for Fourier filtering

The use of two different lens objectives for Fourier filtering, the telecentric lens and the regular objective with an inserted aperture, enables a comparison between the two. In Figure 30, the MTF:s from images taken by the two systems through the 2, 3 and 4 cm cuvettes using green illumination are compared. The key feature is how steep the frequency cut-off is for the two systems. The figures show that the regular objective consistently give a sharper cut-off frequency. One possible reason is that the telecentric lens is located closer to the sector star than the regular objective in the used setup. As explained in sections 3.3 and 6.1, the divergent beam and the use of the sector star causes smoothing of the cut-off. If the Fourier filtering done by the aperture, and corresponding mechanism in the telecentric lens, is not applied exactly at the Fourier plane further smoothing is introduced. The results confirm that a telecentric lens can be used as a low pass filter but suggests that the filtering is not applied at the Fourier plane. Observe that the exact cut-off frequency may vary slightly between the two, as they have been adjusted independently.

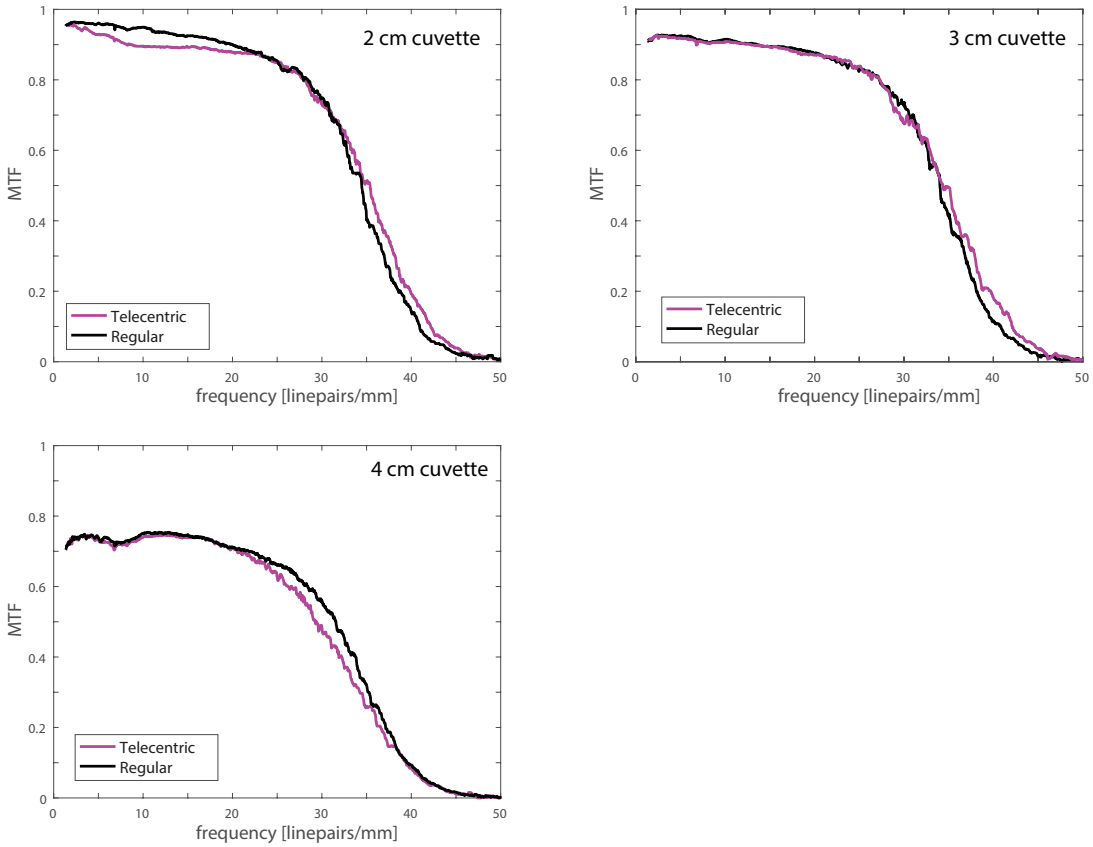

Figure 30: Comparison between MTF:s of FF imaging with a regular objective with an aperture and with a telecentric lens. The graphs show the MTF:s from images recorded at optical depths of 5.01, 7.52 and 10.03.

8 Multi-Scat Monte Carlo simulation

The first part of this section describes some key features of the Multi-Scat software[1] together with the input parameters required by the numerical model. It also explains the attributes of the imaging systems that can or cannot be simulated. The second part shows an MTF comparison between the experimental and the simulated results.

8.1 The Multi-Scat software

The Multi-Scat software uses the Monte Carlo method to simulate photon packets from a source of light propagating through a cubic medium containing spherical particles. The software also simulates a lens collecting the light exiting the medium and forming a final image. The software accepts a user uploaded image representing the light source. The cubic medium, the uploaded source and the geometry of a simulation are shown in Figure 31, as presented by the software. The wavelength, the size of the particles, the refractive indices of the particles and of the surrounding medium, the optical depth and the distance to and size of the lens are all user defined properties. This enables a simulation to closely match an experimental case.

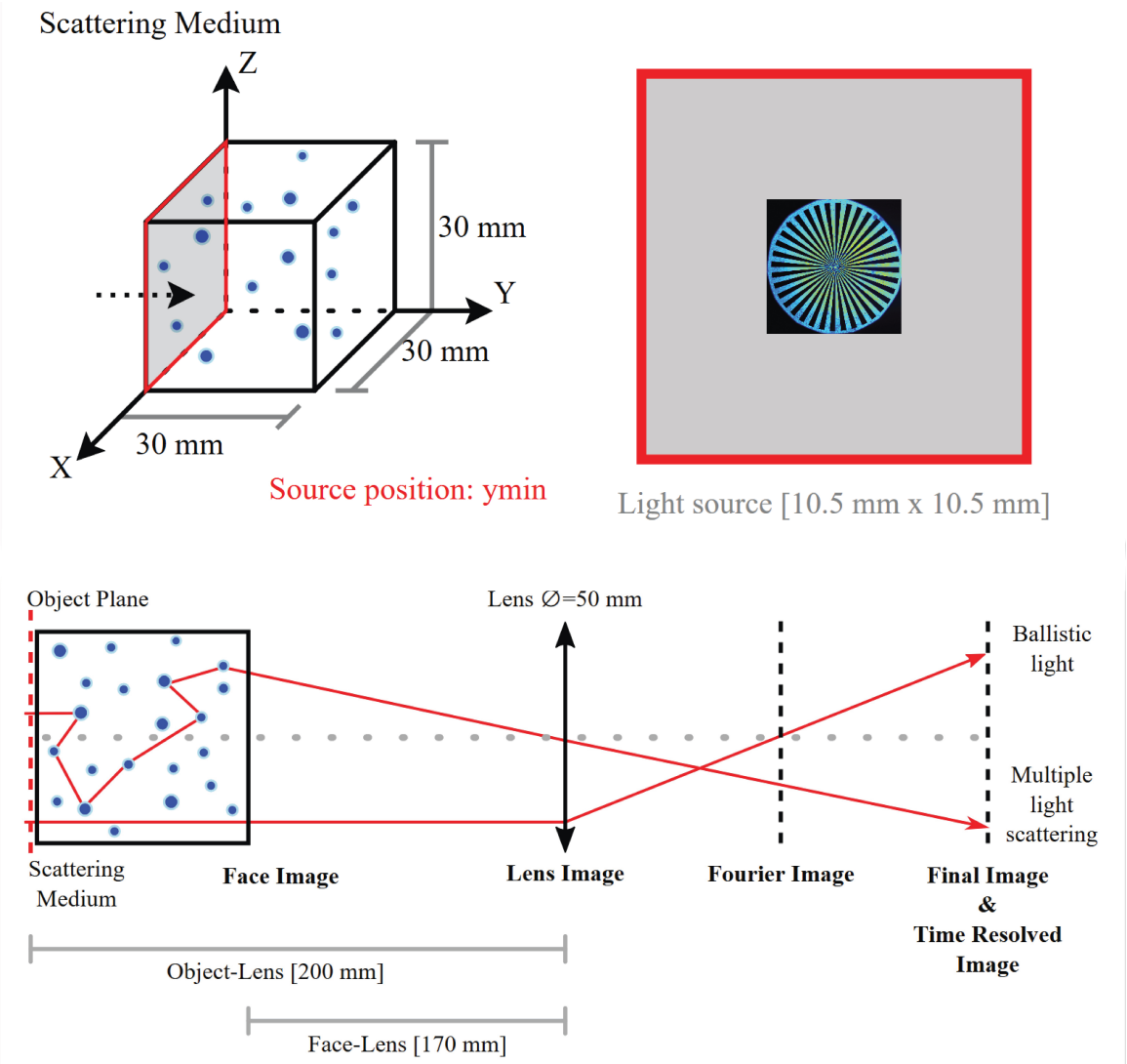

Figure 31: Cubic scattering medium and image light source used in the simulation. Image taken from the software [1].

The software uses the refractive indices and size of the particles to calculate scattering phase functions, such as shown in Figures 1a-1f. When a photon packet leaves the medium, the angle decided by its last interaction in the medium, together with the point of exit, decides whether or not the packet is collected by a virtual lens. Photons collected by the lens may be disregarded if they arrive in at a steeper angle than a threshold angle defined by the user. This feature can be used to mimic the optical Fourier filtering process by choosing the angle corresponding to the acceptance angle of the aperture in the experimental setup.

Some of the optical features in this project cannot be replicated in the simulation. The simulation assumes that the incoming light source is perfectly collimated, which is not the case in the experiment. The simulation also does not take the Fourier components of the light source into account. For this reason, when filtering angles using the simulation, it will not affect high frequencies in the image. When simulating Fourier filtering this can be solved by using an optically Fourier filtered image as a light source. This way, all effects are accounted for but implemented in the reversed order. However, the combined effect on the MTF should be similar.

8.2 Input parameters of the simulation

For the simulations, a new set of images of the sector star was recorded which includes the full surrounding beam. The new set of images were recorded with the blue illumination($\lambda = 473$ nm) through the 3 cm cuvette, using the same scattering medium as above. The images were recorded with two exposure times, 0.01s and 0.1s. Comparison between the two exposure times shows the effect of different signal strength, a property which is difficult to match in the simulation. Images recorded through clean water was used as the input light sources in the simulations. By using images recorded by the experimental setup without the scattering medium, all conditions except for the scattering itself is accounted for.

The properties of the scattering medium described in section 6.1 was used. The properties are listed in Figure 32, as presented in the software. A lens of D = 50 mm at distance 200 mm from the sector star is used, matching the geometry of the regular objective in the experimental setup. The geometry of the simulation is the geometry shown in Figure 31. The acceptance angle in the Fourier filtering is set to 0.86°, corresponding to a lens of focal length $f = 100$ mm with an aperture opening of D= 3 mm. For comparison, data of an acceptance angle of 2° is also saved. The simulation data is saved with the same resolution, 1000×1000, as the amount of pixels of the camera. For each simulation, 10^{12} photon packets are sent.

Total Number of Photons	P_{nb}	=9.99999799296e+5 million
Wavelength	λ	=473 nm
Optical Depth	OD	=11.25
Averaged Scat. Event	S_{nb}	=13.28289
Particle Diameter	$\varnothing_p$	=0.13 μm
Number Density	N	=5.64951552e+8 #/mm³
Light Path Length	L	=30 mm
Extinction Coefficient	μ_e	=0.375 mm⁻¹
Scattering Coefficient	μ_s	=0.3675569 mm⁻¹
Absortion Coefficient	μ_a	=0.007443119 mm⁻¹
Medium Absortion Coeff.	μ_{ma}	=0 mm⁻¹
Particle Refractive Index	n_p	=1.587-0.0004i
Medium Refractive Index	n_m	=1.333-0.0i
Extinction Cross-Section	σ_e	=6.637738e-10 mm²
Scattering Cross-Section	σ_s	=6.50599e-10 mm²
Absortion Cross-Section	σ_a	=1.317479e-11 mm²

Figure 32: Optical properties used in the simulations, as presented by the software [1].

8.3 Simulation validation

The experimental and simulated images are presented in Figure 33. The figure shows simulated and experimental versions of all filtering setups: unfiltered, SI, FF and SIF. The experimental images in the figure are recorded with 0.01s exposure time. The signal in the simulated images are approximately one order of magnitude lower than in the experimental images. The simulated FF image in the figure is the 0.86° acceptance angle case.

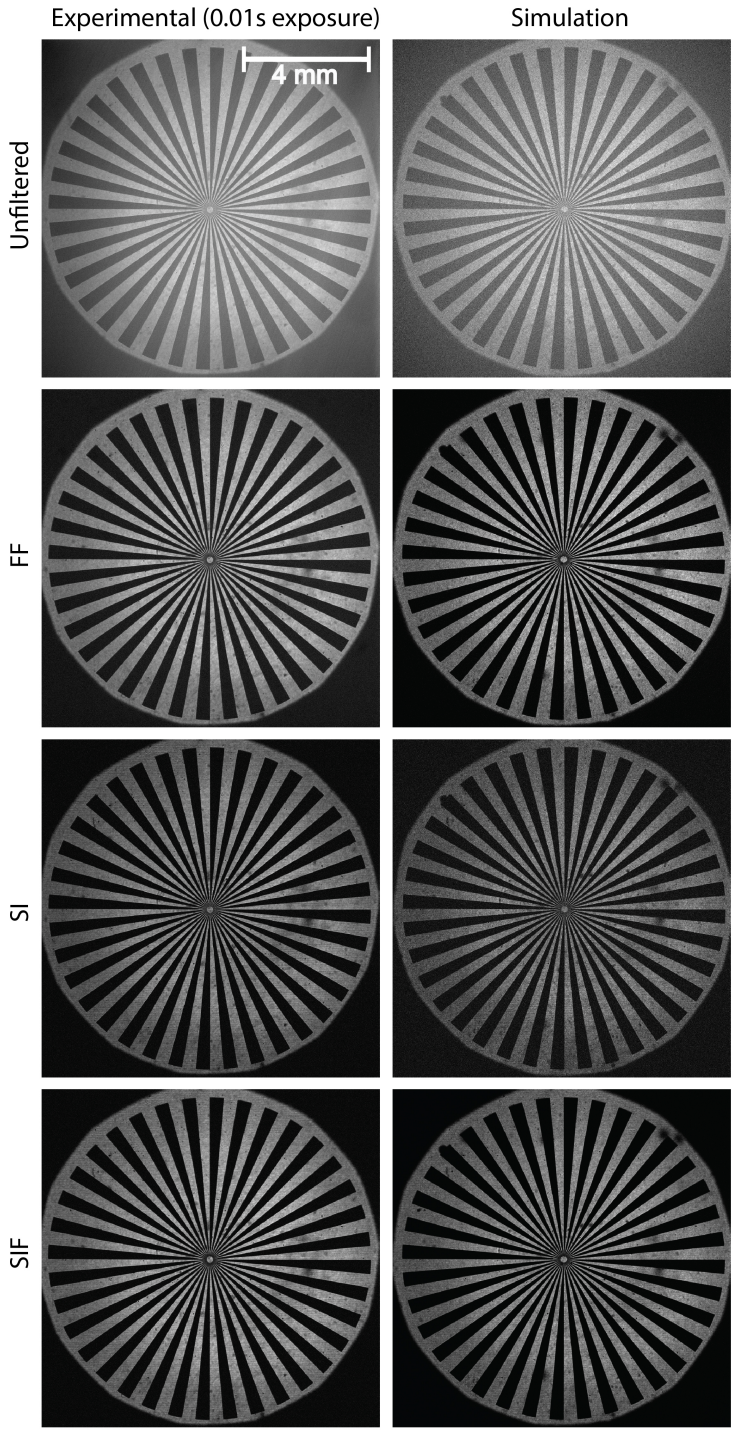

Figure 33: Experimental unfiltered, SI, FF and SIF images recorded through the 3cm cuvette with blue illumination, and corresponding simulated images.

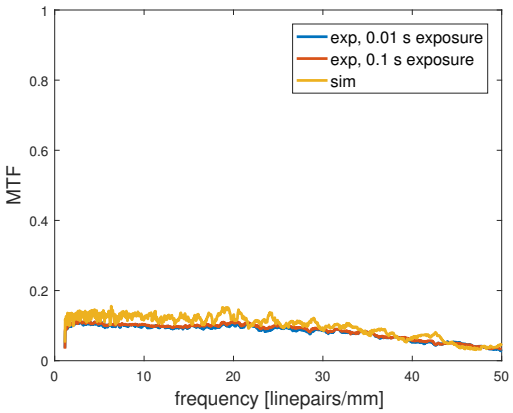

(a) MTF of unfiltered images

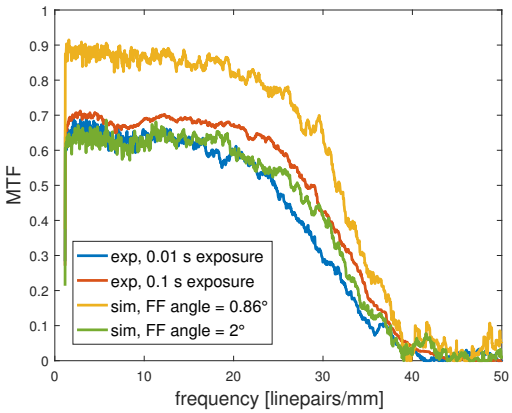

(b) MTF of FF images

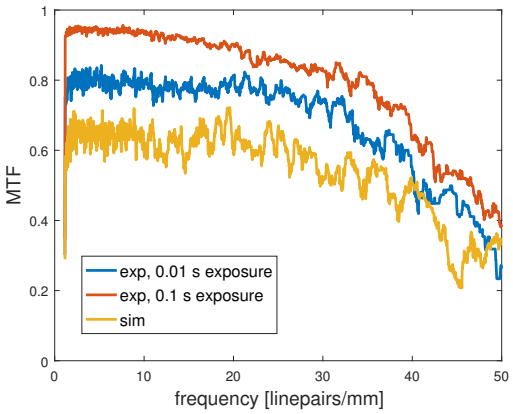

(c) MTF of SI images

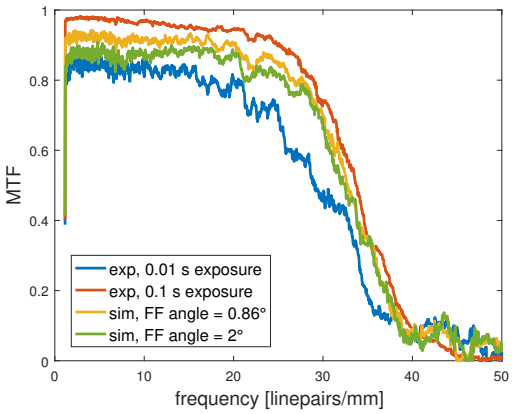

(d) MTF of SIF images

Figure 34: MTF of simulated and experimental imaging with blue($\lambda = 473$ nm) illumination through a 3 cm cuvette.

Figure 34a shows that the simulated and experimental images have very similar contrast. The two experimental exposure times yield almost identical MTF, suggesting that difference in signal is not a major influence in this case. Figure 34b shows the MTF of experimental FF imaging with two exposure times and simulated imaging with different acceptance angles. The experimental acceptance angle corresponds to 0.86°. In this case, an increase in signal does yield an increase in MTF. However, the simulation, with less signal, has the higher contrast. As mentioned above the simulation assumes a perfectly collimated beam. As explained in subsection 3.3, Fourier filtering is more effective for a collimated beam and could be the cause of this difference. The simulation with 2° acceptance angle show that less effective Fourier filtering can cause MTF differences of this magnitude. Figure 34c shows the MTF of simulated and experimental SI imaging. In this case, the MTF shows high sensitivity to signal strength. The difference in signal strength and MTF are both approximately the same between the two experimental imaging cases as between the short exposure experimental imaging and the simulation. This indicates that the difference in signal strength does account for the difference in MTF. The SIF imaging MTF:s in Figure 34d show a combination of the differences observed for the SI and FF simulations. The signal strength lowers the MTF of the simulation and the more effective FF increases it. Combined, these differences cause the experimental and simulated MTF to be relatively similar.

The similar contrast of the simulation and experimental images without optical filtering filtering(34a) show great promise for a full validation of the Multi-Scat software. The other examples show that

the software can be used to simulate optical filtering, but only of a highly collimated beam and with an exact match of the illumination intensity. Multiple simulations with the same amount of photon packets as the ones presented here could be added to match the signal strength of the experiment. Unfortunately this could not be done within the time frame of this project, since the software has been under development and the hardware capable of simulations of this magnitude has only recently been assembled.

9 Conclusions and outlook

In this project an MTF Matlab code, capable of calculating the full and partial angular MTF of an imaging system from an image of a sector star was developed. Two versions of the code implements two different calculation approaches. The calculation of the MTF using a Fourier transform approach does not yield the same result as when using the direct definition. In some situations, the Fourier transform approach provides MTF values higher than unity and shows an unexpected increase in MTF with frequency. Calculation of the MTF should therefore be done from the direct estimation of the minimum and maximum values.

A new optical SIF setup has been developed during this project. The mounted setup illustrated in Figure 19 has more functionality for real world applications than the previously suggested setup. The investigations of this project have concluded that a telecentric lens can be used for Fourier filtering and as a component in SIF. However, the telecentric lens performs slightly worse than the objective-aperture setup originally proposed for SIF [10]. This can be explained as the filtering aperture is positioned as close as possible to the Fourier plane of the objective lens, which is not the case for the telecentric lens.

The measurement results presented in this thesis provide further knowledge of the capabilities of SIF imaging, especially its performance through scattering media of particles smaller than the wavelength. More specifically, the results show that SIF is capable of improving image contrast further than by using Fourier filtering or Structured Illumination individually. The technique is capable of retrieving up to 30% contrast in situations where conventional imaging gives no visibility at all. SIF is especially useful at optical depths higher than 10, where the weaknesses of SI are compensated for by the strengths of FF. The results show that at low optical densities($0 < \mathrm{OD} \leq 5$) all three filtering achieves above 90% contrast. At medium optical densities($5 < \mathrm{OD} \leq 10$) SI and SIF perform equally well and both provide superior contrast than FF. At high optical densities($\mathrm{OD} > 15$), SIF is superior to both SI and FF. The benefit of using SIF over FF gets larger with increasing optical depth, as observed for $\mathrm{OD} = 11.25$ and $\mathrm{OD} = 15$.

The results of this project also provide a deeper knowledge on SIF imaging with different illumination wavelengths. The comparison between different wavelengths(473 nm, 532 nm and 671 nm) through the same scattering medium shows that SIF image contrast remains the same despite the difference in cross-section. When illuminating through a thicker scattering medium the result could not be replicated. Here, blue illumination did not yield the same contrast as the longer wavelengths. The limited power of the illuminating laser could not produce an optimized signal intensity at the camera array. Further investigation is required to conclude if higher power illumination could, with SIF, lead to high visibility imaging at optical depths above 15. A comparison between different wavelengths through the same optical depth also shows that SIF give equal image contrast despite unfiltered contrast difference due to different scattering phase functions.

Further development of the SIF setup includes the use of a higher power laser to investigate the performance of SIF in higher optical densities. Future work should also investigate the effects of scattering media with larger particles on SIF performance.

Finally, an attempt to replicate the experimental results by using the new Multi-Scat software[1] has been made. The software is capable of emulating most aspects of the experimental imaging. The comparison show great promise for the software, as the simulated and experimental imaging have

very similar MTF. However, simulations of imaging with optical filtering techniques(FF, SI and SIF) differ in contrast from the experimental cases. This is likely due to the difference in illumination intensity and beam divergence, which the results show that the MTF is very sensitive to. To further validate the software, future attempts to match the experimental and simulated signal strengths and beam divergence should be made.

Acknowledgements

First and foremost, I want to thank my supervisor Dr. Edouard Berrocal for all his help and support during this project and for sharing his office with me. I also want to thank Mr. Joakim Jönsson for his hard work to make the simulation comparisons possible. A special thanks also goes to Dr. Sven-Göran Petterson who offered his expertise in the development of my MTF code.

Appendices

A MTF comparison for all imaged cases

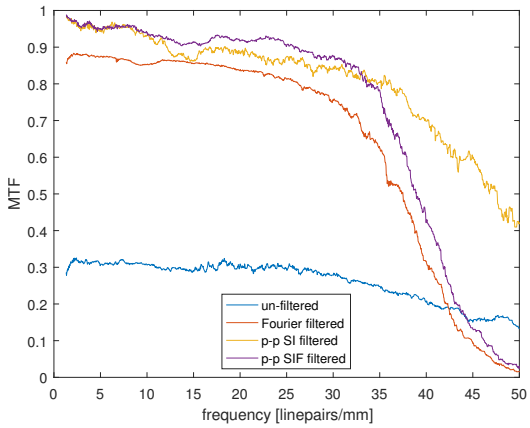

(a) Objective with aperture

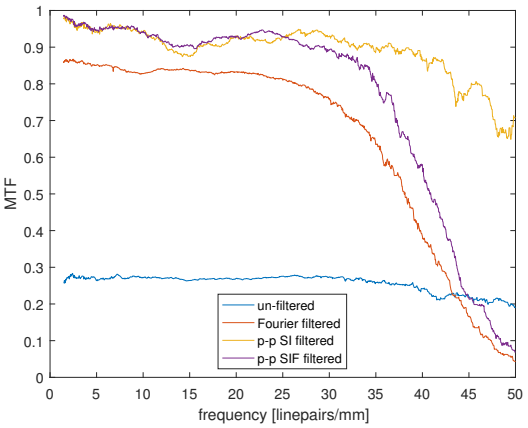

(b) Telecentric lens

Figure A.1: MTF:s for imaging through 2 cm of 0.13 µm diameter particles using blue light.

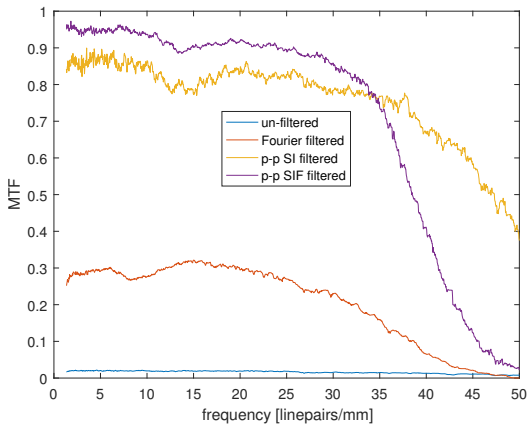

(a) Objective with aperture

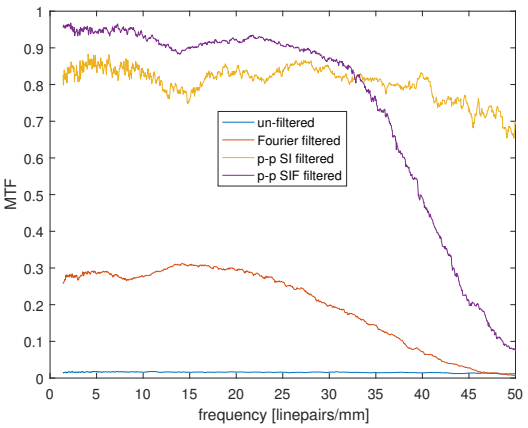

(b) Telecentric lens

Figure A.2: MTF:s for imaging through 3 cm of 0.13 µm diameter particles using blue light.

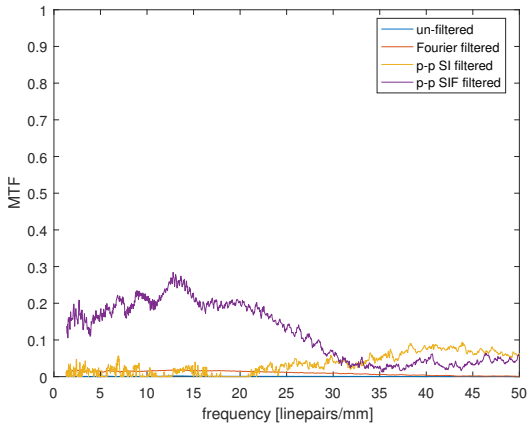

(a) Objective with aperture

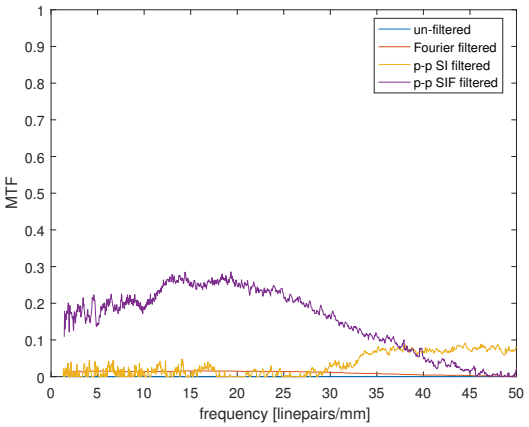

(b) Telecentric lens

Figure A.3: MTF:s for imaging through 4 cm of 0.13 µm diameter particles using blue light.

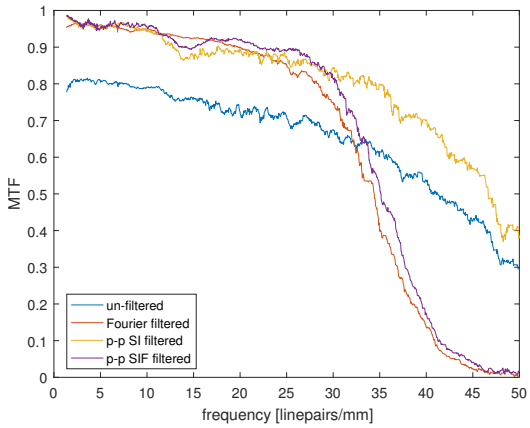

(a) Objective with aperture

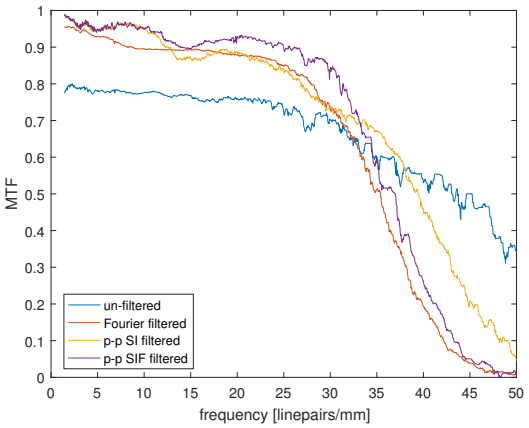

(b) Telecentric lens

Figure A.4: MTF:s for imaging through 2 cm of 0.13 µm diameter particles using green light.

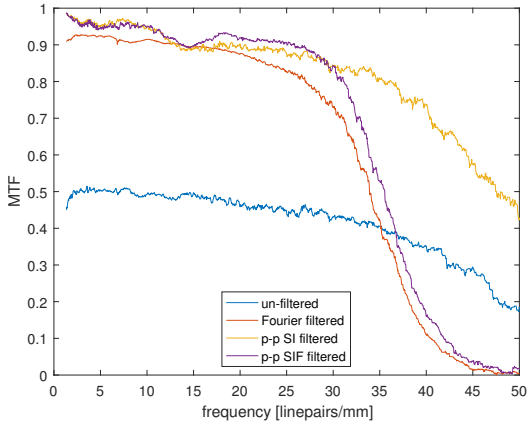

(a) Objective with aperture

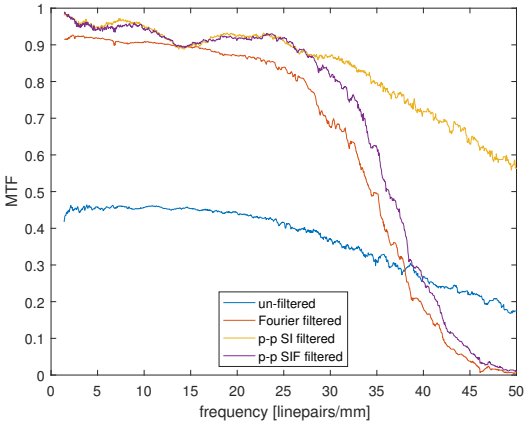

(b) Telecentric lens

Figure A.5: MTF:s for imaging through 3 cm of 0.13 µm diameter particles using green light.

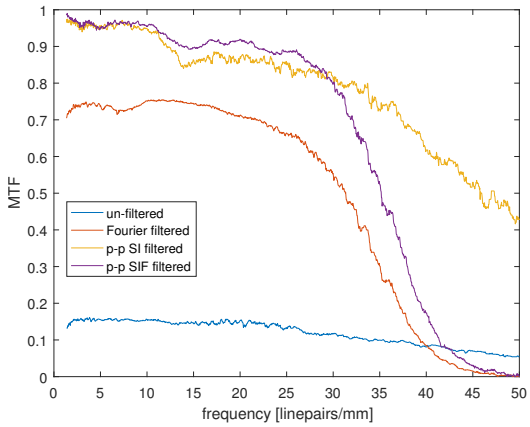

(a) Objective with aperture

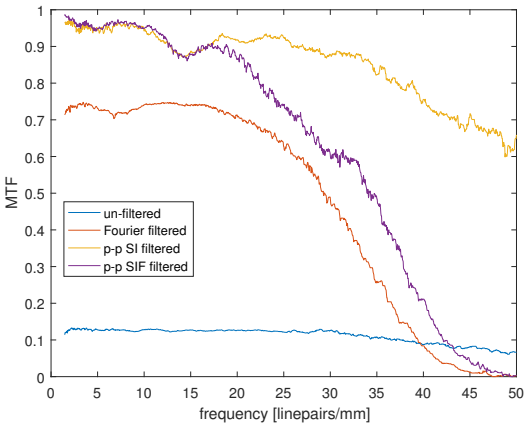

(b) Telecentric lens

Figure A.6: MTF:s for imaging through 4 cm of 0.13 µm diameter particles using green light.

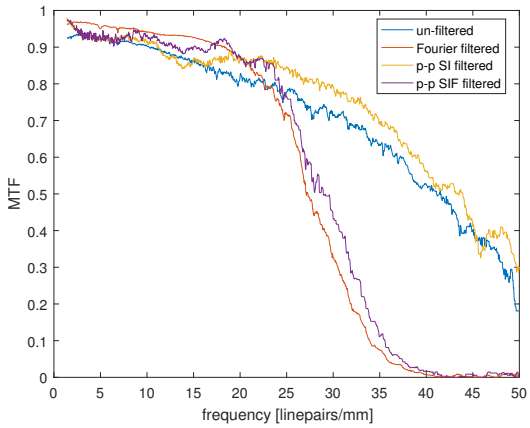

(a) Objective with aperture

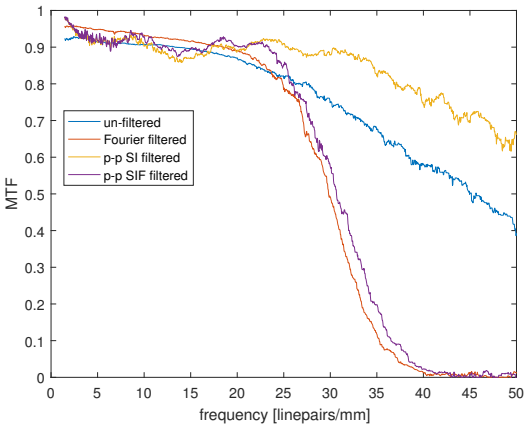

(b) Telecentric lens

Figure A.7: MTF:s for imaging through 2 cm of 0.13 µm diameter particles using red light.

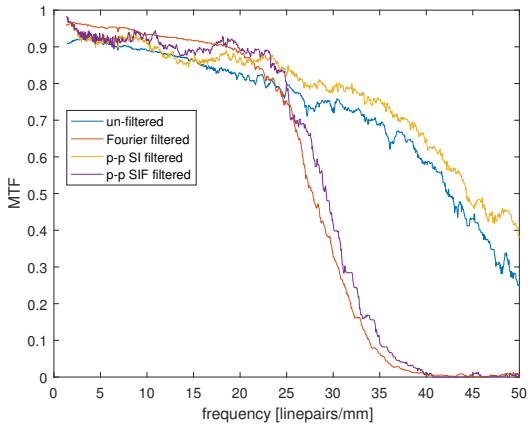

(a) Objective with aperture

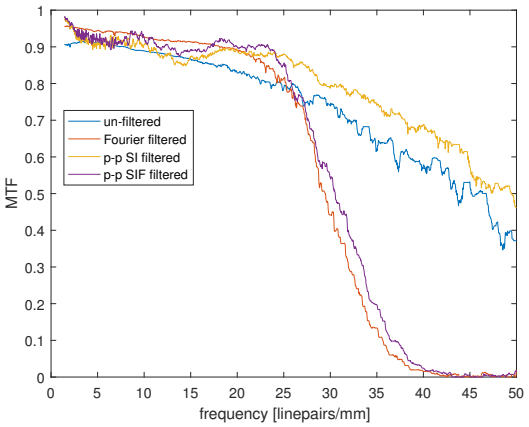

(b) Telecentric lens

Figure A.8: MTF:s for imaging through 3 cm of 0.13 µm diameter particles using red light.

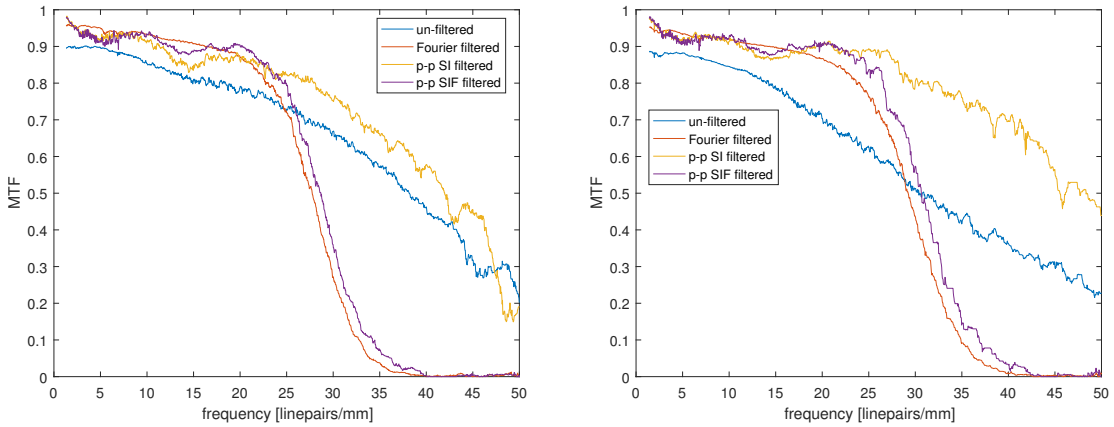

(a) Objective with aperture

(b) Telecentric lens

Figure A.9: MTF:s for imaging through 4 cm of 0.13 µm diameter particles using red light.

B Mathematics of Structured Illumination

This appendix contain a trigonometric proof that any modulation of frequency $n \times f_{mod}$ yields a constant using Eq.5 if phase shifts of $\frac{2\pi}{3}$ and $\frac{4\pi}{3}$ for f_{mod} are used.

An image of intensity I(x,y) is modulated with sinusoidal modulations. Three phase shifted images are defined as:

$$\begin{cases} I_0 = I(x,y) \times [1 + sin(xnf_{mod})] \\ I_{120} = I(x,y) \times [1 + sin(n(xf_{mod} + \frac{2\pi}{3})] \\ I_{240} = I(x,y) \times [1 + sin(n(xf_{mod} + \frac{4\pi}{3})] \end{cases}$$

Where $n \in \mathbb{N}$. Frequencies $n \times f_{mod}$ are phase shifted $n \times \frac{2\pi}{3}$ and $n \times \frac{4\pi}{3}$.

$$\sqrt{(I_0 - I_{120})^2 + (I_0 - I_{240})^2 + (I_{120} - I_{240})^2} =$$

$$= \sqrt{\left(I(x,y) \times [1 + sin(xnf_{mod})] - I(x,y) \times [1 + sin(n(xf_{mod} + \frac{2\pi}{3}))]\right)^2 + ...}$$
$$\overline{\left(I(x,y) \times [1 + sin(xnf_{mod}))] - I(x,y) \times [1 + sin(n(xf_{mod} + \frac{4\pi}{3}))]\right)^2 + ...}$$
$$\overline{\left(I(x,y) \times [1 + sin(n(xf_{mod} + \frac{2\pi}{3}))] - I(x,y) \times [1 + sin(n(xf_{mod} + \frac{4\pi}{3}))]\right)^2} =$$

$$= \sqrt{\left(I(x,y) \times sin(xnf_{mod}) - I(x,y) \times sin(n(xf_{mod} + \frac{2\pi}{3}))\right)^2 + ...}$$
$$\overline{\left(I(x,y) \times sin(xnf_{mod}) - I(x,y) \times sin(n(xf_{mod} + \frac{4\pi}{3}))\right)^2 + ...}$$
$$\overline{\left(I(x,y) \times sin(n(xf_{mod} + \frac{2\pi}{3})) - I(x,y) \times sin(n(xf_{mod} + \frac{4\pi}{3}))\right)^2} =$$

$$= I(x,y) \times \sqrt{\left(sin(xnf_{mod}) - sin(n(xf_{mod} + \frac{2\pi}{3}))\right)^2 + ...}$$
$$\overline{\left(sin(xnf_{mod}) - sin(n(xf_{mod} + \frac{4\pi}{3}))\right)^2 + ...}$$
$$\overline{\left(sin(n(xf_{mod} + \frac{2\pi}{3})) - sin(n(xf_{mod} + \frac{4\pi}{3}))\right)^2} =$$

$$= \sqrt{2} \times I(x,y) \times \sqrt{sin^2(xnf_{mod}) + sin^2(n(xf_{mod} + \frac{2\pi}{3})) + sin^2(n(xf_{mod} + \frac{4\pi}{3})) + ...}$$
$$\overline{-sin(xnf_{mod})sin(n(xf_{mod} + \frac{2\pi}{3})) - sin(xnf_{mod})sin(n(xf_{mod} + \frac{4\pi}{3})) + ...}$$
$$\overline{-sin(n(xf_{mod} + \frac{2\pi}{3}))sin(n(xf_{mod} + \frac{4\pi}{3}))} =$$

Using the trigonometric identity

$$\begin{cases} Asin(x+\Phi) = asin(x) + bcos(x) \\ A = \sqrt{a^2+b^2} \\ a = Acos(\Phi) \\ b = Asin(\Phi) \end{cases}$$

we obtain:

$$\begin{aligned} =\sqrt{2} \times I(x,y) \times \sqrt{sin^2(xnf_{mod}) + \left(cos(\frac{2\pi n}{3})sin(nxf_{mod}) + sin(\frac{2\pi n}{3})cos(nxf_{mod})\right)^2 + ...} \\ \overline{\left(cos(\frac{4\pi n}{3})sin(nxf_{mod}) + sin(\frac{4\pi n}{3})cos(nxf_{mod})\right)^2 + ...} \\ \overline{-sin(xnf_{mod})\left(cos(\frac{2\pi n}{3})sin(nxf_{mod}) + sin(\frac{2\pi n}{3})cos(nxf_{mod})\right) + ...} \\ \overline{-sin(xnf_{mod})\left(cos(\frac{4\pi n}{3})sin(nxf_{mod}) + sin(\frac{4\pi n}{3})cos(nxf_{mod})\right) + ...} \\ \overline{-\left(cos(\frac{2\pi n}{3})sin(nxf_{mod}) + sin(\frac{2\pi n}{3})cos(nxf_{mod})\right)\left(cos(\frac{4\pi n}{3})sin(nxf_{mod}) + sin(\frac{4\pi n}{3})cos(nxf_{mod})\right)} = \end{aligned}$$

$$\begin{aligned} =\sqrt{2} \times I(x,y) \times \sqrt{sin^2(xnf_{mod}) + cos^2(\frac{2\pi n}{3})sin^2(nxf_{mod}) + sin^2(\frac{2\pi n}{3})cos^2(nxf_{mod}) + ...} \\ \overline{+2cos(\frac{2\pi n}{3})sin(nxf_{mod})sin(\frac{2\pi n}{3})cos(nxf_{mod}) + cos^2(\frac{4\pi n}{3})sin^2(nxf_{mod}) + ...} \\ \overline{+sin^2(\frac{4\pi n}{3})cos^2(nxf_{mod}) + 2cos(\frac{4\pi n}{3})sin(nxf_{mod})sin(\frac{4\pi n}{3})cos(nxf_{mod}) + ...} \\ \overline{-cos(\frac{2\pi n}{3})sin^2(xnf_{mod}) - sin(\frac{2\pi n}{3})cos(nxf_{mod})sin(xnf_{mod}) + ...} \\ \overline{-cos(\frac{4\pi n}{3})sin^2(xnf_{mod}) - sin(\frac{4\pi n}{3})cos(nxf_{mod})sin(xnf_{mod}) + ...} \\ \overline{-cos(\frac{2\pi n}{3})sin(nxf_{mod})cos(\frac{4\pi n}{3})sin(nxf_{mod}) - cos(\frac{2\pi n}{3})sin(nxf_{mod})sin(\frac{4\pi n}{3})cos(nxf_{mod}) + ...} \\ \overline{-sin(\frac{2\pi n}{3})cos(nxf_{mod})cos(\frac{4\pi n}{3})sin(nxf_{mod}) - sin(\frac{2\pi n}{3})cos(nxf_{mod})sin(\frac{4\pi n}{3})cos(nxf_{mod})} = \end{aligned}$$

We now observe that

$$cos(\frac{2\pi n}{3}) = cos(\frac{4\pi n}{3}) = \begin{cases} -\frac{1}{2}, & \text{for } n = 1,4,7... \\ -\frac{1}{2}, & \text{for } n = 2,5,8... \\ 1, & \text{for } n = 3,6,9... \end{cases}$$

$$sin(\frac{2\pi n}{3}) = -sin(\frac{4\pi n}{3}) = \begin{cases} \frac{\sqrt{3}}{2}, & \text{for } n = 1,4,7... \\ -\frac{\sqrt{3}}{2}, & \text{for } n = 2,5,8... \\ 0, & \text{for } n = 3,6,9... \end{cases}$$

enabling pair-wise cancellation of

$$sin(\frac{2\pi n}{3})cos(nxf_{mod})sin(xnf_{mod}) \quad \text{against} \quad sin(\frac{4\pi n}{3})cos(nxf_{mod})sin(xnf_{mod})$$

and

$$sin(\frac{2\pi n}{3})cos(nxf_{mod})cos(\frac{4\pi n}{3})sin(nxf_{mod}) \quad \text{against} \quad sin(\frac{4\pi n}{3})cos(nxf_{mod})cos(\frac{2\pi n}{3})sin(nxf_{mod})$$

leaving:

$$\sqrt{(I_0 - I_{120})^2 + (I_0 - I_{240})^2 + (I_{120} - I_{240})^2} =$$

$$= \sqrt{2} \times I(x,y) \times \sqrt{sin^2(xnf_{mod}) + cos^2(\frac{2\pi n}{3})sin^2(nxf_{mod}) + sin^2(\frac{2\pi n}{3})cos^2(nxf_{mod}) + ...}$$

$$\overline{+cos^2(\frac{4\pi n}{3})sin^2(nxf_{mod}) + sin^2(\frac{4\pi n}{3})cos^2(nxf_{mod}) - cos(\frac{2\pi n}{3})sin^2(xnf_{mod}) - cos(\frac{4\pi n}{3})sin^2(xnf_{mod}) + ...}$$

$$\overline{-cos(\frac{2\pi n}{3})sin(nxf_{mod})cos(\frac{4\pi n}{3})sin(nxf_{mod}) - sin(\frac{2\pi n}{3})cos(nxf_{mod})sin(\frac{4\pi n}{3})cos(nxf_{mod})} =$$

We further observe that

$$\begin{cases} cos(\frac{2\pi n}{3})cos(\frac{4\pi n}{3}) = cos^2(\frac{2\pi n}{3}) \\ \\ cos^2(\frac{2\pi n}{3}) = cos^2(\frac{4\pi n}{3}) \end{cases} ; \quad \begin{cases} sin(\frac{2\pi n}{3})sin(\frac{4\pi n}{3}) = -sin^2(\frac{2\pi n}{3}) \\ \\ sin^2(\frac{2\pi n}{3}) = sin^2(\frac{4\pi n}{3}) \end{cases}$$

which simplifies the expression to

$$\sqrt{(I_0 - I_{120})^2 + (I_0 - I_{240})^2 + (I_{120} - I_{240})^2} =$$

$$= \sqrt{2} \times I(x,y) \times \sqrt{sin^2(xnf_{mod}) + cos^2(\frac{2\pi n}{3})sin^2(nxf_{mod}) + ...}$$

$$\overline{3sin^2(\frac{2\pi n}{3})cos^2(nxf_{mod}) - 2cos(\frac{2\pi n}{3})sin^2(xnf_{mod})} =$$

$$= \sqrt{2} \times I(x,y) \times \sqrt{\left(1 + cos^2(\frac{2\pi n}{3}) - 2cos(\frac{2\pi n}{3})\right) sin^2(xnf_{mod}) + 3sin^2(\frac{2\pi n}{3})cos^2(nxf_{mod})} =$$

$$= \sqrt{2} \times I(x,y) \times \sqrt{sin^2(xnf_{mod}) \begin{cases} \frac{9}{4}, & \text{for } n = 1,4,7... \\ \frac{9}{4}, & \text{for } n = 2,5,8... \\ 0, & \text{for } n = 3,6,9... \end{cases} + cos^2(nxf_{mod}) \begin{cases} \frac{9}{4}, & \text{for } n = 1,4,7... \\ \frac{9}{4}, & \text{for } n = 2,5,8... \\ 0, & \text{for } n = 3,6,9... \end{cases}} =$$

which, by the trigonometric identity

$$sin^2(x) + cos^2(x) = 1$$

yields

$$\sqrt{(I_0 - I_{120})^2 + (I_0 - I_{240})^2 + (I_{120} - I_{240})^2} = I(x,y) \times \begin{cases} \frac{3}{\sqrt{2}}, & \text{for } n \neq 3,6,9... \\ \\ 0, & \text{for } n = 3,6,9... \end{cases}$$

Hence, any higher order of the fundamental frequency f_{mod} yields a constant times $I(x,y)$. $\square$

References

[1] J. Jönsson and E. Berrocal. Multi-scat (beta) [online software]. `http://ff-desk029.forbrf.lth.se:27014`, 2017.

[2] E. Hecht. *Optics, Global Edition, Fifth Edition.* Pearson Education, Harlow, England, 2017.

[3] H. C. van de Hulst. *Light Scattering by Small Particles.* Dover Publications, Inc, New York, USA, 1981.

[4] L. Wang, P. P. Ho, X. Liang, H. Dai, and Alfano R. R. Kerr–fourier imaging of hidden objects in thick turbid media. *Optics Letters*, 18, 1993.

[5] D. Sedarsky, E. Berrocal, and M. Linne. Quantitative image contrast enhancement in time-gated transillumination of scattering media. *Optics Express*, 19, 2011.

[6] H. Ramachandran and S. Mujumdar. Imaging through turbid media using polarization modulation: dependence on scattering anisotropy. *Optics Communications*, 241, 2004.

[7] Q. Z. Wang, X. Liang, L. Wang, P. P. Ho, and Alfano R. R. Fourier spatial filter acts as a temporal gate for light propagating through a turbid medium. *Optics Letters*, 20, 1995.

[8] H. Ramachandran and A. Narayanan. Two-dimensional imaging through turbid media using a continuous wave light source. *Optics Communications*, 154, 1998.

[9] E. Berrocal, J. Johnsson, E. Kristensson, and M. Alden. Single scattering detection in turbid media using single-phase structured illumination filtering. *Journal of the European Optical Society - Rapid publications*, 7(0), 2012.

[10] E. Berrocal, S. Pettersson, and E. Kristensson. High-contrast imaging through scattering media using structured illumination and fourier filtering. *Optics Letters*, 41, 2016.

[11] E. Berrocal. *Multiple Scattering of Light in Optical Diagnostics of Dense Sprays and Other Complex Turbid Media.* PhD thesis, Cranfield University, 2006.

[12] E. Kristensson. *Structured Laser Illumination Planar Imaging(SLIPI) - Applications for Spray Diagnostics.* PhD thesis, Lund University, 2012.

[13] B. E. A. Saleh and M. C. Teich. *Fundamentals of Photonics, Second Edition.* John Wiley and Sons, Inc, Hoboken, USA, 2007.

[14] The advantages of telecentricity. `https://www.edmundoptics.com/resources/application-notes/imaging/advantages-of-telecentricity/`. Accessed: 2017-06-05.

[15] X. Ma, J. Q. Lu, R. S. Brock, K. M. Jacobs, P. Yang, and X. Hu. Determination of complex refractive index of polystyrene microspheres from 370 to 1610 nm. *Physics in Medicine and Biology*, 48, 2003.